저작자표시-비영리-변경금지 2.0 대한민국

이용자는 아래의 조건을 따르는 경우에 한하여 자유롭게

- 이 저작물을 복제, 배포, 전송, 전시, 공연 및 방송할 수 있습니다.

다음과 같은 조건을 따라야 합니다:

저작자표시. 귀하는 원저작자를 표시하여야 합니다.

비영리. 귀하는 이 저작물을 영리 목적으로 이용할 수 없습니다.

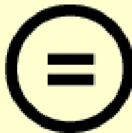

변경금지. 귀하는 이 저작물을 개작, 변형 또는 가공할 수 없습니다.

- 귀하는, 이 저작물의 재이용이나 배포의 경우, 이 저작물에 적용된 이용허락조건을 명확하게 나타내어야 합니다.
- 저작권자로부터 별도의 허가를 받으면 이러한 조건들은 적용되지 않습니다.

저작권법에 따른 이용자의 권리는 위의 내용에 의하여 영향을 받지 않습니다.

이것은 이용허락규약(Legal Code)을 이해하기 쉽게 요약한 것입니다.

Disclaimer

dCollection

工學碩士

The Effect of Seed Layer on the MgO Thin Film Using the Sol-Gel Method on Si(100)

指導教授 金 泓 承

2016 年 8 月

韓國海 洋大學校 大學院

電子材料工學科

楊沂達

本 論文을 楊沂達의

工學碩士 學位論文으로 認准함.

委員長 梁 瑨 (印)

委 員 金 泓 承 (印)

委 員 張 樂 元 (印)

2016年 8月

韓國海洋大學校 大學院

Collection @ kmou

Contents

List of Figures V

List of Tables VII

Abstract VIII

Chapter 1. Introduction ..... - 1 -

Chapter 2. Literature Survey ..... - 3 -

2.1 Introduction of MgO Material ..... - 3 -

2.1.1 The Physical Properties of MgO Materials ..... - 3 -

2.1.2 The Application of MgO Materials ..... - 5 -

2.2 Introduction of ZnO Material ..... - 7 -

2.2.1 The Physical Properties of ZnO ..... - 7 -

2.2.2 Application of ZnO ..... - 9 -

2.3 Introduction of $Mg_xZn_{1-x}O$ Material ..... - 10 -

2.3.1 Structural Properties of $Mg_xZn_{1-x}O$ ..... - 10 -

2.3.2 Application of $Mg_xZn_{1-x}O$ ..... - 12 -

Chapter 3. Experimental and Analysis Methods ..... - 13 -

3.1 The Methods of Preparing MgO Film ..... - 14 -

3.1.1 RF Magnetron Sputtering ..... - 14 -

3.1.2 Sol-Gel ..... - 17 -

3.2 Other Methods ..... - 20 -

3.2.1 Electron-Beam Evaporation (EBM) ..... - 20 -

3.2.2 Molecular Beam Epitaxy (MBE) ..... - 22 -

3.2.3 Metalorganic Vapour Phase Epitaxy (MOVPE) ..... - 24 -

3.2.4 Pulsed laser deposition (PLD) ..... - 25 -

Collection @ kmou

3.4 The Analysis Methods of MgO Film - 26 -

3.4.1 X-ray Diffraction (XRD) - 26 -

3.4.2 Atomic Force Microscopy (AFM) - 30 -

3.4.3 Scanning Electron Microscope (SEM) - 31 -

3.4.4 Energy-dispersive X-ray Spectroscopy (EDX) - 32 -

3.4.5 Transmission Electron Microscopy(TEM) - 33 -

Chapter 4. Results and Discussions - 34 -

4.1 Experiment and Procedure - 34 -

4.2 The Characteristics of the MgO Film Grown on Si(100) Substrate - 37 -

4.2.1 The Analysis of XRD - 37 -

4.2.2 The Analysis of AFM - 42 -

4.2.3 The Analysis of SEM and TEM - 46 -

Chapter 5. Summary and Conclusion - 49 -

Reference - 50 -

Acknowledgement - 54 -

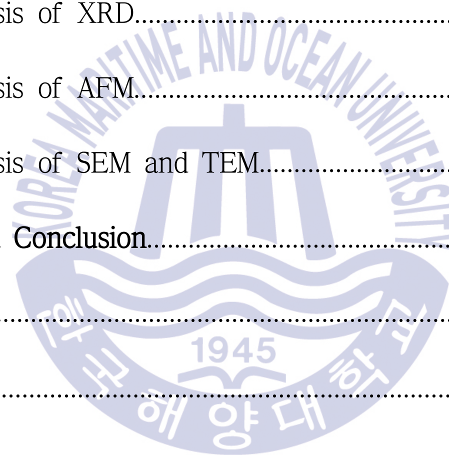

Collection @ kmou

List of Figures

Fig. 1.1 The schematic structure of MgO

Fig. 1.2 The single crystal MgO

Fig. 2.1 Atomic structure of zincblende (a), wurtzite (b) and rocksalt (c) structures. *Closed circle, open circle, and thick solid line* represent cation, anion, and projection of two bonds, respectively

Fig. 2.2 Schematic representation all the application of ZnO mentioned in the text.

Fig. 2.3 The structural models of (a) hexagonal and (b) cubic MgZnO alloys [7]

Fig. 3.1 Sputtering at the molecular level.

Fig. 3.2 The summrized merits of RF megnetron sputtering

Fig. 3.2 Schematic representation of the different stages and routes of the sol-gel technology

Fig. 3.4 The summerized merits of sol-gel method

Fig. 3.5 Schematic representation of E-beam evaporation

Fig. 3.6 Schematic cross-section of a typical MBE growth chamber [48]

Fig. 3.7 Schematics of Bragg's law where d is the interplanar spacing and θ is diffraction angle

Fig. 3.8 Inter-atomic Force vs. distance

Fig. 3.9 AFM scan system

Fig. 3.10 Schematic of the electron and x-ray optics of a combined SEM-EPMA

Fig. 3.11 Principle of EDS measurement

Fig. 3.12 Layout of optical components in a basic TEM

Fig. 4.1 Basic procedure of the experiment. (a) presents the comparison which has no buffer layer compared with (b)

Fig. 4.2 XRD profile of the samples which had different buffer layer annealed at various temperature

Collection @ kmou

Fig. 4.3 XRD profile of samples which were sputtered for 30 mins

Fig. 4.4 FWHM profile of the samples which were annealed at different temperature

Fig. 4.5 The epitaxy relationship between cubic MgO(111) and hexagonal ZnO(0001)

Fig. 4.6 AFM results of the MgO films which were grown on (b) MgO buffer layer, (c) ZnO buffer layer and (d) $Mg_{0.3}Zn_{0.7}O$ buffer layer

Fig. 4.7 3D morphology of MgO thin films which were grown on (b) MgO buffer layer, (c) ZnO buffer layer and (d) $Mg_{0.3}Zn_{0.7}O$ buffer layer

Fig. 4.8 The relation between grain size and RMS

Fig. 4.9 Surface morphology of the samples observed by SEM after annealed at 900℃. The sample (a) and (b) were processed under condition ② as shown in Table 3.2; samples (c) was processed without filter process

Fig. 4.10 The surface of the samples obtained by TEM

Fig. 4.11 The cross section of the samples which were based on (a) MgO buffer layer, (b) ZnO buffer layer and (c) Mg0.3Zn0.7O buffer layer

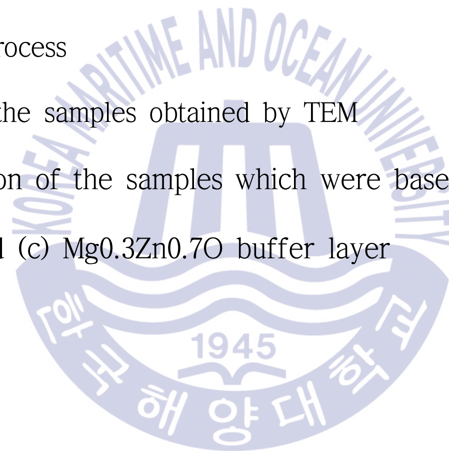

Collection @ kmou

List of Tables

Table 1.1 Properties of MgO material

Table 2.1 Properties of ZnO material

Table 4.1 The parameters of the solution

Table 4.2 The main condition parameters of the experiment

Collection @ kmou

The Effect of Seed Layer on the MgO Thin Film Using the Sol-Gel Method on Si(100)

Yida Yang

Department of Electronic Material Engineering

Graduate School of Korea Maritime and Ocean University

Abstract

MgO film has many excellent physical and chemical properties. It is widely used as the buffer layer and simple protective layer and so many researchers have been attracted by it due to its huge potential in microelectronics field. According to the existing researches, it is found that growing MgO thin film on Si substrate only by RF magnetron sputtering method is very difficult. The growth rate of growing MgO thin film by using this method is very low. As for this experiment, RF magnetron sputtering and so-gel method were combined together to prepare MgO film and obtained a very good result. The structural properties of MgO film were investigated to optimize growth conditions to obtain high quality MgO film. First, RF magnetron sputtering was used to deposit three different dense buffer layers on Si(100) substrate, which were conducted under various growth conditions. Those three different buffer layers referred to MgO buffer layer, ZnO buffer layer and $Mg_{0.3}Zn_{0.7}O$ buffer layer, respectively. Then by using the sol-gel method, the prepared solution was coated on those different buffer layer by using spin coater to obtain MgO film which had a certain thickness. The structure and surface morphology of the samples were characterized by using atomic force microscopy (AFM), X-ray diffraction (XRD), scanning electron microscopy (SEM) and TEM (Transmission electron microscope).

XRD profiles showed that (111) preferred orientation occurred obviously in the XRD

Collection @ kmou

profiles. After annealed at 700 ℃ in oxygen, the MgO film began to crystallize. With the annealing temperature increasing, MgO(111) peak intensity became stronger, while the FWHM became smaller and the crystalline quality of the film was getting better. Compared the MgO film which was prepared only by sol-gel methods, after introducing ZnO and $Mg_{0.3}Zn_{0.7}O$ buffer layer, XRD results showed that the MgO film became much better, while the impact of the introduction of MgO buffer layer film was very weak. Probably due to the low growth rate of MgO film prepared by using RF magnetron sputtering, the MgO buffer layer was too thin or the crystal quality was not good. Those reasons may restrict the effect of the MgO buffer layer. SEM photographs showed that after filtering the solution, the surface of MgO film was very smooth and the phenomenon of surface cracking was reduced significantly. The presence of substances or large insoluble particles existed in the solution can account for it. During spin coating process, these large particles severely affect the uniformity and stability of the film. Furthermore, the coefficient of thermal expansion difference between the particle and the film made such cracking phenomenons occur during the post annealing process. The TEM results showed that the obtained MgO film had dense structure, uniform thickness and a clear boundary over the Si substrates judging by cross-section figures. The diffusion among the Si substrate, buffer layers and the MgO film was not obvious. AFM results showed that the crystalline grain was spherical and crystalline state was obvious. After annealed at a certain temperature limit, the roughness of the surface decreased as the temperature rose. Over the limit, the surface roughness began to increase. As for the grain size, the changes in grain size is inversely related to the change of surface roughness.

KEYWORDS: MgO film, buffer layer, RF magnetron sputtering, sol-gel

Collection @ kmou

Chapter 1. Introduction

In recent years, due to the potential application in the field of microelectronics, oxide films have been widely studied. In order to prepare high-quality oxide film, single-crystal MgO and $SrTiO_3$ material are considered to be the most suitable substrate material. However, widespread use of single crystal of MgO and $SrTiO_3$ which are regarded as the substrate material is not practical because of the expensive cost of these bulk single crystals materials. On the other hand, in order to develop advanced microelectronics, optical and electromagnetic devices, the researches pay much energy on how to integrate Silicon with the ferroelectric [1], the high magnetoresistive oxides [2] and HTS (high-temperature superconductor) which has a perovskite structure [3]. However, some chemical reactions or mutual diffusion between those films and Si substrate could take place easily when the substrate temperature is little too high. That could account for some questions why many functional oxide films cannot be grown directly on Si substrate. Besides, lattice mismatch is an other important reason [4]. It will greatly influence the function of oxide film and the Si substrate, which requires a suitable material to work as a buffer layer to avoid these undesirable phenomena. MgO film has good thermal stability and chemical inertness, which makes it possible to work as a buffer layer for some functional oxide thin films. Meanwhile, MgO films grown on Si substrate can be used as template for epitaxial growth, especially for some oxide thin films which have perovskite structure. Due to its small dielectric constant and low dielectric loss, MgO film has become the excellent materials to make some devices which are based on high-temperature superconductors [5]. In addition, it can also be grown on some other substrates, such as GaAs [6], Al_2O_3 [7,8], Fe [9], Ag [10,11], Mo [12] and so on.

However, MgO film crystal orientation will affect the functional film crystalline orientation and cause some large differences in property due to the anisotropy of the oxides [60]. The surface roughness of the functional thin film will also have a huge impact

Collection @ kmou

on the structure of the film. Preparation of high quality MgO film is the basis and the guarantee to prepare high quality functional oxide films. Currently, there are a lot of methods to prepare MgO film, such as electron beam evaporation (EBM), pulsed laser deposition (PLD), RF magnetron sputtering, metal organic chemical vapor deposition (MOCVD), molecular beam epitaxy (MBE), sol-gel and so on. Due to the low growth rate of growing MgO thin film only by using RF magnetron sputtering, RF magnetron sputtering and sol-gel method were combined together to prepare MgO film in this paper. With the help of X-ray diffraction (XRD), atomic force microscopy (AFM), scanning electron microscopy (SEM) and Transmission electron microscope (TEM), we systematically studied the effects of different buffer layer on the structure properties of MgO film. The purpose is aimed to improve the growth process to prepare MgO film with high quality and less time consumption on Si(100) substrate.

Collection @ kmou

Chapter 2. Literature Survey

2.1 Introduction of MgO Material

MgO material has many excellent physical and chemical properties, such as high thermal stability, high chemical stability, strong anti-sputtering, low dielectric constant, etc. It can be applied in many fields, such as microelectronics period, optical films, plasma display and so on. In recent years, it has attracted more and more researchers for its in-depth study. This chapter will detail the physical and chemical properties of the MgO materials and its applications.

2.1.1 The Physical Properties of MgO Materials

MgO is the metal ionic oxide, with crystal structure of NaCl structure, belongs to the cubic crystal system. It is a Ⅱ-Ⅵ binary compound metal semiconductor. The structure of MgO consists of two interpenetrating fcc lattices of oxygen anions and metal cations in +2 oxidation sate which are held together by ionic bonding, making these oxides even more ionic than prototypical ionic NaCl. The schematic structure and the single crystal MgO are shown in Fig. 1.1 and Fig. 1.2, respectively. At room temperature, the lattice constant a is about 4.21 Å. The band gap E_g is about 7.7eV and usually MgO is insulator. It has a high melting point (about 2800 ℃), which is twice of the Si, and has good thermal stability. The refractive index is about 9.8. The dielectric constant is 1.74 and the refractive index of visible light is above 90%.

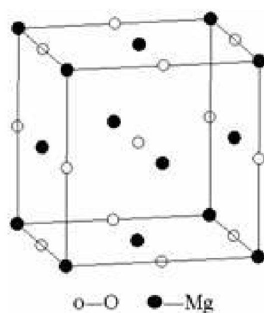

Fig. 1.1 The schematic structure of MgO

Fig. 1.2 The single crystal MgO

Collection @ kmou

MgO is an interesting material being transparent, thermally stable and having high electrical resistivity [13]. It has attracted considerable interest as a material for a broad spectrum of electronic applications ranging from gate insulators in metal-oxide-semiconductor(MOS) transistors to buffer layers enabling integration of other functional oxides [14]. Moreover, MgO can be alloyed with ZnO to control the band gap of ZnO system. The main properties of MgO are summarized in Table 1.1.

Table 1.1 Properties of MgO material

Properties	**Value**
Lattice constant	a=0.4215 nm
Crystal structure at 300K	Cubic rock salt
Band gap energy	7.8 eV
Density	3.576 g/cm^3
Melting point	2 852 ℃
Boiling point	3 600 ℃
Thermal conductivity at 300K	45-60 $W \cdot m^{-1} \cdot K^{-1}$
Thermal Expansion	14 x 10^{-6} K^{-1}
Refractive index	1.736
Dielectric constant	9.83
Linear expansion coefficient (/℃)	10.5×10^{-6}
Transmission Range	0.2 - 8 ㎛
Loss Tangent	3.3 x 10^{-7}
Hardness	5.8 (Mohs)

Collection @ kmou

2.1.2 The Application of MgO Materials

MgO film is widely used in high-temperature superconducting oxides, ferroelectrics, high reluctance oxide buffer layer and TTFT. Used as the buffer layer, MgO film has many excellent features:

(1) Many perovskite oxide can be epitaxially grown on MgO single crystal substrate. MgO film which is grown on a Si substrate could provide a structured template for epitaxial growth of perovskite oxide film.

(2) As for MgO(100) film and the most (100)-oriented perovskites whose the lattice constant is 3.8 Å, the lattice mismatch is about -9.5%. This will bring a huge stress in perovskite oxide thin film, which provides us convenience to study the stress among those oxide films.

(3) We can obtain three kinds of MgO film which has (100), (110) and (111) crystal orientation on Si(100) substrate. It is possible to use them to control the growth orientation of perovskite oxide thin film on Si substrate, which brings us convenience to study the anisotropy of these oxides.

(4) The refractive index is 1.74. Compared with other buffer layer (such as CeO_2 and YSZ), the refractive index is very small, which makes the MgO film ideally suited to be the buffer layer for photoconductive film.

(5) Due to its low dielectric constant and low dielectric loss, MgO thin film is very suitable to be used as a buffer layer for microwave devices which are based on high-temperature superconductors.

MgO film is commonly used as dielectric protective layer for plasma display panel (PDP) [15,16]. Since the plasma display can be used for all digital mode and easy to be made in large-screen display, it became the highly competitive next-generation display device for digital TV, HDTV and multimedia terminal. As a protective layer of the PDP glow

Collection @ kmou

discharge process, MgO film should have the following conditions:① low ignition voltage; ② long lifetime;③ excellent storage performance;④ high transmittance of visible light.

Collection @ kmou

2.2 Introduction of ZnO Material

2.2.1 The Physical Properties of ZnO

Most of the group Ⅱ－Ⅵ binary compound semiconductors crystallize in either cubic zinc blende or hexagonal wurtzite (Wz) structure where each anion is surrounded by four cations at the corners of a tetrahedron, and vice versa. ZnO materials are Ⅱ－Ⅵ compound semiconductor whose iconicity resides at the borderline between covalent and ionic semiconductor [16]. The crystal structure of ZnO includes wurtzite (B4), zinc blende (B3) and rocksalt (B1), as schematically shown in Fig. 2.1 [17]. Under ambient conditions, the thermodynamically stable phase is that of wurtzite symmetry. The zinc blende ZnO structure can be stabilized only by growth on cubic substrates, and the rocksalt or Rochelle salt (NaCl) structure may be obtained at relatively high pressures, as in the case of GaN [16].

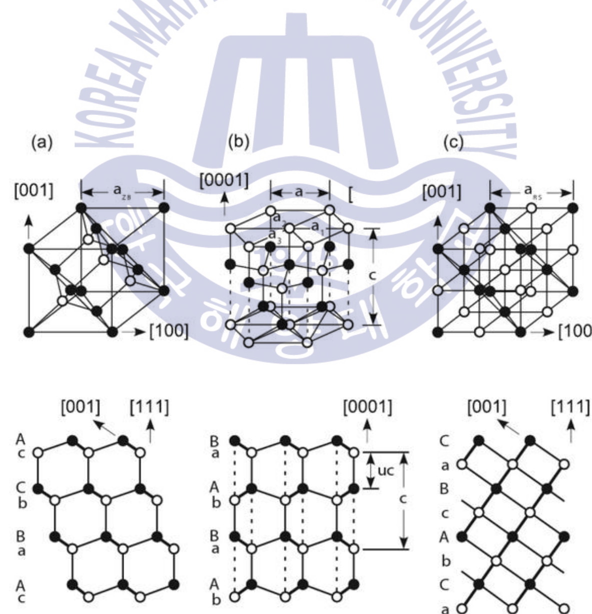

Fig. 2.1 Atomic structure of zincblende (a), wurtzite (b) and rocksalt (c) structures. *Closed circle, open circle, and thick solid line* represent cation, anion, and projection of two bonds, respectively

The ZnO with wurtzite structure which is composed of two interpenetrating hexagonal-close-packed (hcp) sublattices is the thermodynamically stable phase at ambient conditions. The hexagonal crystal structure with a=3.24Å and c=5.12Å belongs to the space group of P63mc. And along the [0001] direction in Fig. 2.1(b), the Zn cation and O anion

Collection @ kmou

connected by dashed lines attract each other by electrostatic force. That is why the hexagonal wurtzite ZnO resides at the borderline between covalent and ionic semiconductor.

ZnO is a wide bandgap and direct band compound semiconductor. The valence band(VB) of pure ZnO is formed by the Zn-3*d* states and the O-2*p* states, and the conduction band (CB) is mainly formed by the 4*s* sates of Zn and the 2*s* states of O. Moreover, the conduction band minimum (CBM) and the valence band maximum(VBM) are formed by Zn-4*s* states and the O-sp states [18]. The band gap width of ZnO is 3.37 eV and can be tuned via divalent substitution on the cation site. For example, the replacement of Zn by Mg increase the band gap to ~3.0 eV [19]. The total physical properties of ZnO are shown in Table 2.1.

Table 2.1 Properties of ZnO material

Properties	Value
Lattice parameter at 300K a_0 c_0 c_0/a_0	 0.32495 nm 0.52069 nm 1.602 (ideal value = 1.6333)
u	0.345
Density	5.606 g/cm^3
Stable phase at 300K	Wurtzite
Melting temperature	1975 ℃
Linear expansion coefficient (/℃)	a_0: 6.5×10^{-6} c_0: 3.0×10^{-6}
Static dielectric constant	8.656
Refractive index	2.008, 2.029
Energy band gap	3.4 eV, direct
Intrinsic carrier concentration	$< 10^6$ cm^{-3}
Exciton binding energy	60 meV
Electron effective mass	0.24
Electron hall mobility at 300K for n-type conductivity	200 cm^2/Vs
Hole effective mass	0.59
Hole hall mobility at 300K for low p-type conductivity	5-50 cm^2/Vs

Collection @ kmou

2.2.2 Application of ZnO

Because of its diverse properties, both chemical and physical, zinc oxide is widely used in many areas. It plays an important role in a very wide range of applications, ranging from tyres to ceramics, from pharmaceuticals to agriculture, and from paints to chemicals. Due to the direct and wide band gap, ZnO is suited to be applied in blue and UV optical devices. Moreover, ZnO has large excitation binding energy about 60 meV (GaN ~ 22 meV), which makes the ZnO optical device to be expected more effective to the emitting efficiency than the GaN optical devices [20,21]. Because of its large piezoelectric constant, ZnO is able to be used in some applications, such as voltage generates, sensors, transducers and actuators. It also can be used for sensor devices due to its strong sensitivity of surface conductivity to the presence of adsorbed species [22]. In the Fig. 2.2, summarized application paths of ZnO are presented.

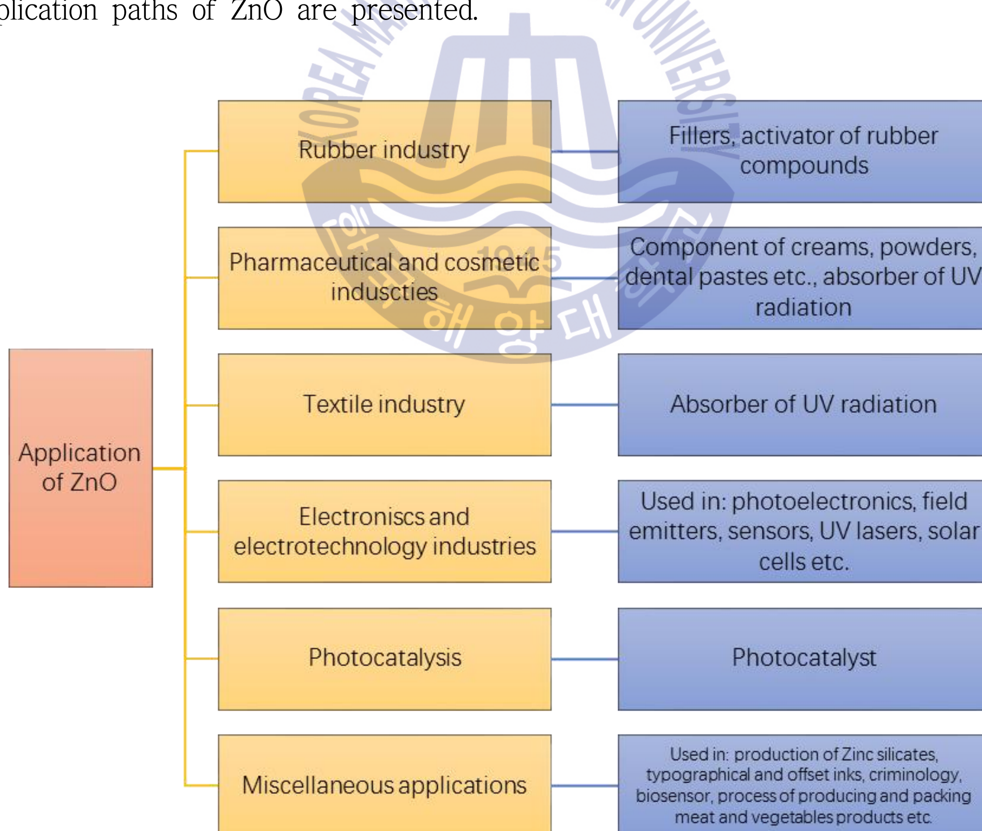

Fig. 2.2 Schematic representation all the application of ZnO mentioned in the text.

Collection @ kmou

2.3 Introduction of $Mg_xZn_{1-x}O$ Material

2.3.1 Structural Properties of $Mg_xZn_{1-x}O$

It is possible for ternary semiconducting crystals to smoothly change many important physical properties by varying their composition [23,24,25]. Ternary $Mg_xZn_{1-x}O$ alloy is a ZnO and MgO solid solution material. Since the ionic radius of Mg^{2+}(0.57 A) is close to that of Zn^{2+} (0.6 A), the replacement of Zn atom by Mg atom should not cause a significant change of the lattice constant. However, a large crystal structure dissimilarity between the wurtzite-hexagonal ZnO and the rock-salt-cubic MgO can cause unstable phase mixing [26]. $Mg_xZn_{1-x}O$ may have a hexagonal or cubic lattice structure depending on the different growth conditions.

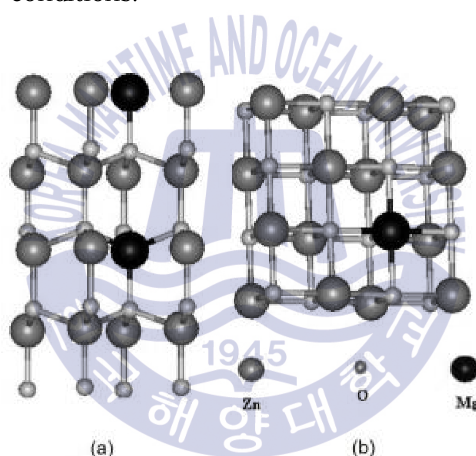

Fig. 2.3 The structural models of (a) hexagonal and (b) cubic MgZnO alloys [7]

Despite the similarity between Zn^{2+} and Mg^{2+} ionic radii, the thermodynamic solubility limit of MgO in ZnO is less than 4 at.% [27]. In 1998, Ohtomo *et al.* [28] have fabricated $Mg_xZn_{1-x}O$ films by PLD and the hexagonal structure was maintained to 33 at.%, which presented the possibility of growing wurtzite $Mg_xZn_{1-x}O$ films with high Mg content. In 2003, Takeuchi *et al.* [29] have fabricated $Mg_xZn_{1-x}O$ films by PLD at substrate temperature of 600℃ and found the phase separation region of the phase diagram in the range of $0.37 \leq x \leq 0.6$. However, L.K.Wanga *et al.* [30] have grew the cubic MgZnO layer with x=0.33 by using MOCVD technique. The stability of material depends on the difference between the total energies of cubic and hexagonal lattice structures, and also depends on

Collection @ kmou

temperature because the total energy of different lattice structures changes at different rates with the changing temperature [31].

Collection @ kmou

2.3.2 Application of $Mg_xZn_{1-x}O$

$Mg_xZn_{1-x}O$ with tunable bandgap from 3.37 eV to 7.8 eV, which covers a broad portion of the ultraviolet spectrum, is a promising candidate for the applications in UV optoelectronic devices such as light emitting diodes, ultraviolet (UV), photodetectors (PDs) and photovoltaic (PV) devices [32-34]. ZnO is a promising optoelectronic material in the field of ultraviolet-light-emitting devices and laser diodes, owing to its wide band gap and high exciton binding energy at room temperature. In order to get high illumination intensity and improve the illumination efficiency, $Mg_xZn_{1-x}O$/ZnO heterojunction is widely used.

$Mg_xZn_{1-x}O$ thin films have high transmittance in the visible region and high electrical conductivity which can be easily controlled by doping. It can be applied for electrode and window material of solar cells. What's more, it's an ideal candidate for the application of solar cells which can be equipped on space satellites result from its lower damage of irradiation in high-irradiation environments [35]. In addition, $Mg_xZn_{1-x}O$ can also be used in piezoelectric devices, such as voltage generates, sensors, transducers and actuators, owing to its large piezoelectric constant [36].

Collection @ kmou

Chapter 3. Experimental and Analysis Methods

Currently, there are many methods to prepare MgO film, such as beam evaporation (EBM), pulsed laser deposition (PLD), RF magnetron sputtering, metal organic chemical vapor deposition (MOCVD), molecular beam epitaxy (MBE), sol-gel method (sol-gel), etc.. Different methods have different characteristics and they will affect the properties of MgO film, such as crystal orientation, surface roughness, compactness and so on. Different applications have different requirements of the film quality, which need to use corresponding methods of preparation to obtain suitable film. Of course, there are many analysis methods to test the performance of the prepared films, such as X-ray diffraction (XRD), reflection high-energy electron diffraction (RHEED), atomic force microscopy (AFM), scanning electron microscopy (SEM) and so on. In this chapter, the basic principles advantages or shortcomings of those various preparation methods will be introduced . The effects of process conditions for the film properties will be discussed. At the same time, some brief introductions of testing the characterization of MgO film are also mentioned.

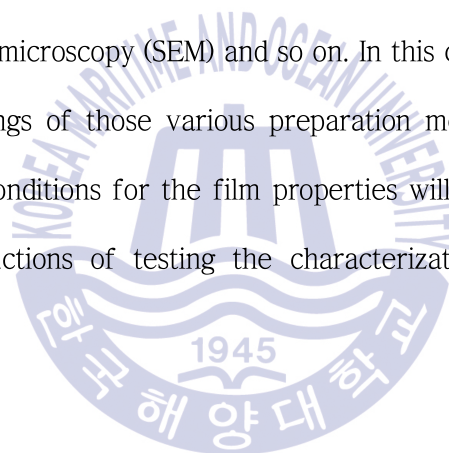

Collection @ kmou

3.1 The Methods of Preparing MgO Film

3.1.1 RF Magnetron Sputtering

RF Magnetron Sputtering is based on the theory that particle to particle collisions will involve an elastic transfer of momentum, which can be utilized to apply a thin film to the substrate. In this technique, ions are accelerated toward a target by utilizing electric fields. These ions are usually derived from either an ion gun or from exciting a neutral gas into ion plasma. As the ions are accelerated and bombard the target surface, they dislodge target atoms and other ions. The ejected atoms attach themselves to the substrate, and a thin film of the target material is produced [38].

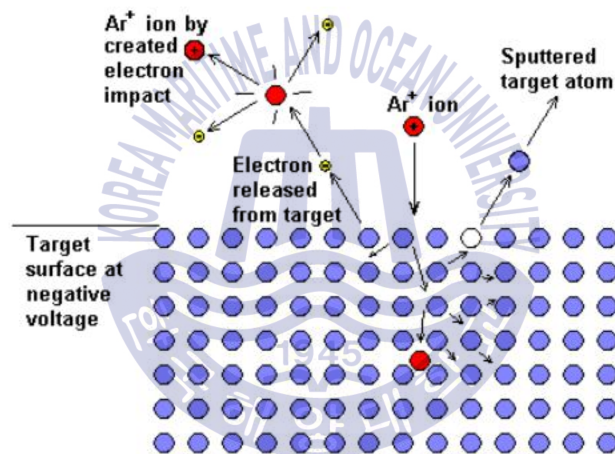

Fig. 3.1 Sputtering at the molecular level

Fig. 3.1 shows the schematic representation of sputtering at the molecular level. Magnetron sputtering can be done either in DC or RF modes which depend on the conductivity of the target material. If the target material is a conductor, a constant voltage can be used to accelerate the ions to the desired bombarding velocity. As the ions strike the surface, the resulting charges can move freely about the material to prevent any charge buildup. However, RF magnetron sputtering can be done both conducting and non-conducting materials. As for insulator, the conduction bands will not allow free charge movement. Here, magnets are used to increase the percentage of electrons that take part in ionization of events and thereby increase the probability of electrons striking the

Collection @ kmou

Argon atoms, increase the length of the electron path, and hence increase the ionization efficiency significantly. As the ions strike the surface, their charge will remain localized and over time the charge will build up, making it impossible to further bombard the surface. In order to prevent this, alternating current is used at a frequency above 50 KHz. A high frequency is used so that the heavy ions cannot follow the switching fast enough and only electrons hit the surface to neutralize charge [38]. The merits of the RF magnetron sputtering are summerized in Fig. 3.2.

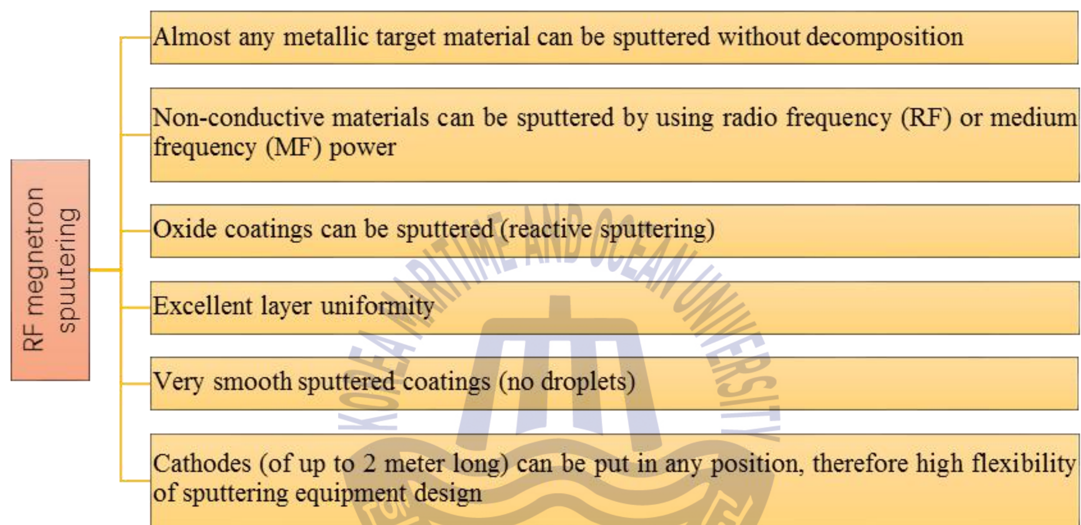

Fig. 3.2 The summrized merits of RF megnetron sputtering

Jung Heon Lee *et al.* [39] showed that Changing the deposition conditions could change the characteristics of the film. With increasing operating pressure, the crystallinity was deteriorated and the surface roughness was reduced. While increasing the film density, the grain size was substantially constant. While the grain size and surface roughness became larger and film density became smaller as RF power increasing. They Also pointed out that the hydration of MgO film was impacted by film density and grain size. R.Soto *et al.* [40] adopted DC magnetron sputtering method to grow MgO film and the results showed that the deposition rate was influenced by discharge power and the oxygen content. They successfully increased the productive rate and yield better MgO films. Furthermore, they resolved the phenomenon of frequent spark discharge when MgO was adopted as

Collection @ kmou

target. Kyung H. Nam *et al.* [41] added two grids between the target and the substrate to modify the traditional magnetron sputtering system. The result showed that the improved magnetron sputtering system could produce higher density plasma than conventional magnetron sputtering system. The MgO film synthesized by this improved system had a dense structure and smooth surface.

Collection @ kmou

3.1.2 Sol-Gel

Sol-Gel refers to a process in which solid nanoparticles dispersed in a liquid (a sol) agglomerate together to form a continuous three-dimensional network extending throughout the liquid (a gel). At the first stage of the sol-gel process the hydrolysis and polycondensation reactions lead to the formation of a colloidal solution, i.e. sol, of hydroxide particles whose size does not exceed several dozen nm. Increasing bulk concentration of the dispersed phase or other changes in external conditions (pH, solvent substitution) leads to the intense formation of contacts between particles and the formation of a monolithic gel, in which the solvent molecules are enclosed in a flexible, but fairly stable, three-dimensional grid formed by particles of hydroxides. Concentration of sols followed by gelation is carried out using dialysis, ultrafiltration, electrodialysis, evaporation at relatively low temperatures, or extraction.

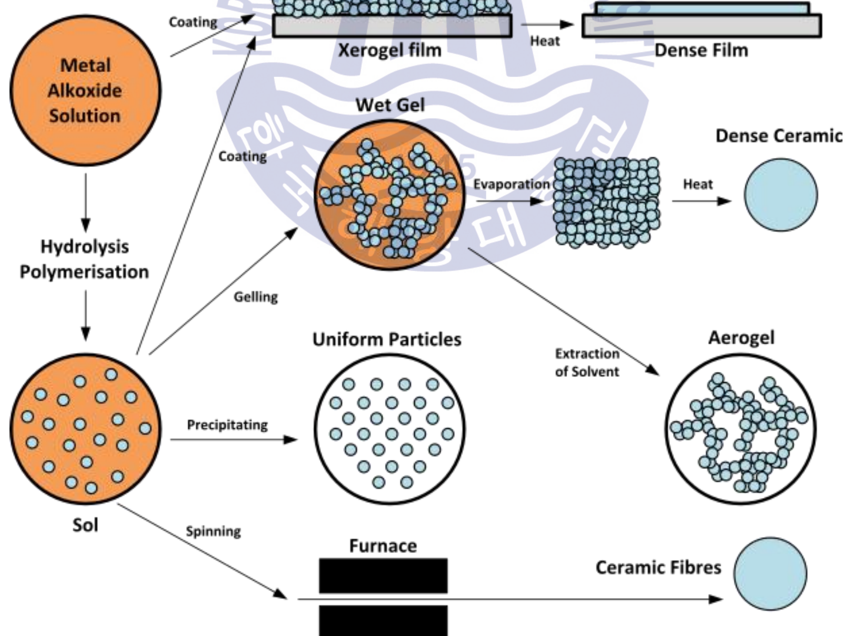

Fig. 3.3 Schematic representation of the different stages and routes of the sol-gel technology

By adjusting the viscosity of the sol, we can deposit the solution on the substrate by spin coating, dip coating and spraying to obtain the wet film. After drying to remove the solvent, you can get the dry film. After high-temperature treatment, the organic

Collection @ kmou

component in the film will be removed and an amorphous inorganic film is obtained. If you want to obtain a crystal film, high temperature annealing process is necessary, which is relying on high temperature diffusion of atoms nucleating crystallization.

All in all, the basic process involves 5 stages: source material, sol, gel, heat treatment and materials. Due to its excellent characteristics, such as the high purity and good uniformity Stoichiometry can also be precisely controlled. Due to the low temperature and easy operation, sol-gel has become widely used method for producing an inorganic film. In addition, drying and annealing are fatal factors for the film preparation. The organic component cannot be fully removed if drying or annealing temperature is too low. If the temperature is too high, gel will shrink so fast that the film surface will become uneven or crack. Jong-Gul Yoon *et al.* [54] pointed out that because the formation of the thin film is the solid-phase crystallization during heat treatment which is accompanied by undesirable chemical reactions in this stage. That resulted in an oxide layer or other intermediate phase. It is very difficult to epitaxially grow excellent oxide film on a semiconductor substrate.

The basic principles of sol-gel method are described as follows [42] :

(1) Solvation: in the ionizable precursor, metal salts, M^{Z+} metal cation attracts water molecules to form a solvent unit, $M(H_2O)_nZ^+$ (Z is the valence of M ions). In order to balance its strong coordination number, it has a strong trend to release H^+:

$$M(H_2O)_nZ+ \longleftrightarrow M(H_2O)_{(Z-1)} + H^+$$

while if some other ions are added into this system, it is possible to produce a condensation reaction. But the formula will become extremely complex.

(2) Hydrolysis reaction: Non-ionizing molecular precursors, such as metal alkoxides $M(OR)_n$ (n is the valence of the metal M), will react with water:

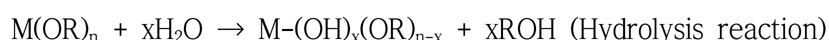

$$M(OR)_n + xH_2O \rightarrow M\text{-}(OH)_x(OR)_{n-x} + xROH \text{ (Hydrolysis reaction)}$$

dCollection @ kmou

(3) After the hydrolysis, dehydration condensation reaction and dealcoholization condensation reaction can form anhydrous oxide network structure. The particles can have various sizes and structures.

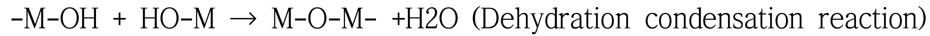
-M-OH + HO-M → M-O-M- +H2O (Dehydration condensation reaction)

-M-OH + RO-M → M-O-M- +ROH (Dealcoholization condensation reaction)

The summerized merits of sol-gel method is shown in Fig. 3.4.

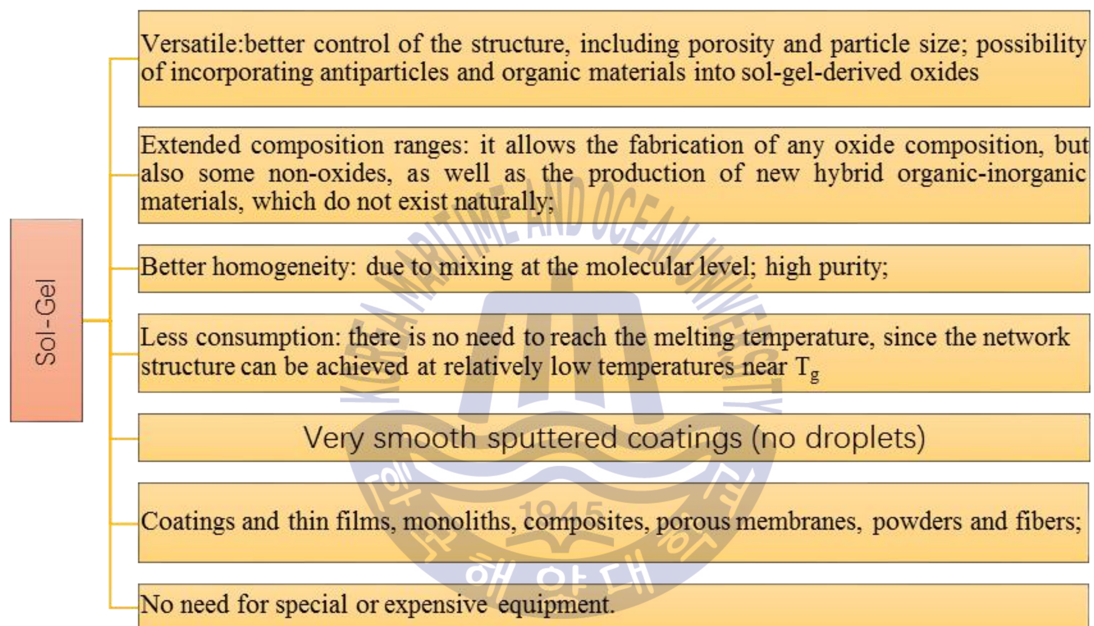

Fig. 3.4 The summerized merits of sol-gel method

Jnog—Gul Yoon *et al.* [54] successfully used sol-gel method to obtain MgO(111) film on Si(111) and Si(100). The results showed that the film crystal orientation was not determined by the substrate crystal orientation. While it was easier to obtain MgO(111) film on Si(111) substrate because they have similar crystal orientation. At the same time, the crystallinity maybe be affected by the dosage of collodion and the annealing temperature [43,59].

Collection @ kmou

3.2 Other Methods

3.2.1 Electron-Beam Evaporation (EBM)

E-Beam Evaporation is a process similar to thermal evaporation, i.e. a source material is heated above its boiling/sublimation temperature and evaporated to form a film on the surfaces that is stroke by the evaporated atoms. This evaporation method has just like thermal evaporation a pore ability to cover steps which also makes this method ideal for lift-off processes. A noticeable advantage of e-beam evaporation over thermal evaporation is the possibility to add a larger amount of energy into the source material. This yields a higher density film with an increased adhesion to the substrate. Because the electron beam only heats the source material and not the entire crucible, a lower degree of contamination from the crucible will be present than in the case of thermal evaporation. By using a multiple crucible E-beam gun, several different materials can be deposited without breaking the vacuum.

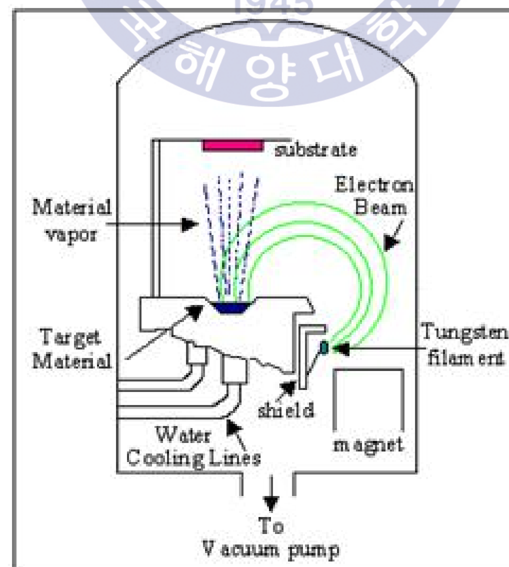

Fig. 3.5 Schematic representation of E-beam evaporation

Collection @ kmou

The E-beam evaporation process is summarized as following:

(1) With the source material placed in the crucible a filament below the crucible is heated;

(2) By applying a large voltage, electrons are drawn from the filament and focused as a beam on the source material by several bending magnets.;

(3) The beam is swept across the surface of the source material to heat all of the material.

When using this method to prepare MgO film, the substrate temperature has a huge influence on the film structure and the surface morphology. Jeong Soo Lee *et al.* [44] grew the MgO(111) film on SiO_2/Si substrate. The results showed that (111) orientation was the preferred orientation, while (100) orientation became stronger with the annealing temperature increasing. TEM results showed that the film had very good grain in the early growth stages, which had the columnar grain structure and the average grain size at the surface was about 40nm. T.W.Kim *et al.* [45,46] obtained MgO(110) films which had smooth and dense structure on p-GaAs(100) and p-InP(100) substrate at corresponding temperature of 250℃ and 200℃, respectively. The results showed that the mismatch between film and the GaAs substrate was the main problem when the temperature was below 250℃. When the temperature was over 450℃, the diffusion was very obvious. As for InP substrate, the similar problem occurred 150℃ and 350℃. The surface roughness of the film was 2~3 nm and the growth rate was 0.06~0.2 nm/s. Akira Sugawara *et al.* [47] obtained homoepitaxial MgO film on MgO(110) substrate and the corresponding growth rate was 7.2 nm/min. They found the surface morphology varied with the deposition temperature. In short, using the method of electron beam evaporation can grow good MgO film with high-quality at a lower temperature and a lower degree of vacuum.

Collection @ kmou

3.2.2 Molecular Beam Epitaxy (MBE)

Molecular Beam Epitaxy (MBE) is a process for growing thin, epitaxial films of a wide variety of materials, ranging from oxides to semiconductors to metals. It was first applied to the growth of compound semiconductors. That is still the most common usage in large part because of the high technological value of such materials to the electronics industry. In this process beams of atoms or molecules in an ultra-high vacuum environment are incident upon a heated crystal that has previously been processed to produce a nearly atomically clean surface. The arriving constituent atoms form a crystalline layer in registry with the substrate, i.e., an epitaxial film. These films are remarkable because the composition can be rapidly changed, producing crystalline interfaces that are almost atomically abrupt. Thus, it has been possible to produce a large range of unique structures, including quantum well devices, superlattices, lasers, etc., all of which benefit from the precise control of composition during growth. Because of the cleanliness of the growth environment and the precise control over composition, MBE structures closely approximate the idealized models used in solid state theory [48]. The schematic of a typical MBE growth chamber is shown in Fig. 3.6.

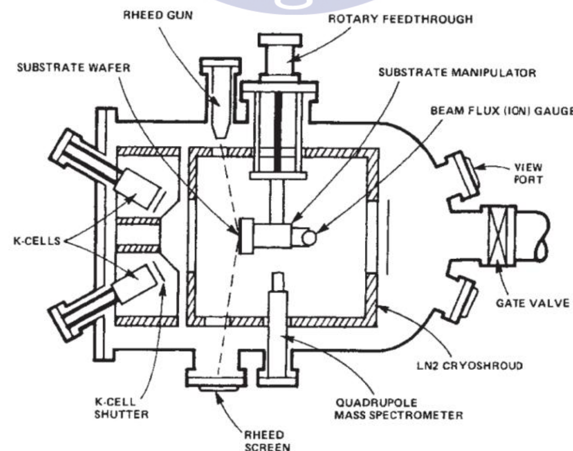

Fig. 3.6 Schematic cross-section of a typical MBE growth chamber [48]

Using MBE technique, we can grow some ultrathin films which has high crystallinity

Collection @ kmou

and smooth surface. Augs Setiwana *et al.* [49] prepared MgO film by using plasma enhanced MBE(P-MBE) in order to provide a buffer layer for ZnO film. They found that the MgO film which was grown at a low temperature (490℃) had atomic scale surface roughness and the dislocation density was decreased. So the quality of ZnO film was greatly improved.

Collection @ kmou

3.2.3 Metalorganic Vapour Phase Epitaxy (MOVPE)

Metalorganic vapour phase epitaxy (MOVPE), also known as organometallic vapour phase epitaxy (OMVPE) or metalorganic chemical vapour deposition (MOCVD), is a chemical vapour deposition method used to produce single or polycrystalline thin films. It is a much higher throughput technique compared with MBE, and as such is the production deposition tool of choice for most compound semiconductor devices such as High Brightness LED's (HBLED). The principle of MOCVD is quite simple. Atoms that you would like to be in your crystal are combined with complex organic gas molecules and passed over a hot semiconductor wafer. The heat breaks up the molecules and deposits the desired atoms on the surface, layer by layer. By varying the composition of the gas, you can change the properties of the crystal at an almost atomic scale. It can grow high quality semiconductor layers (as thin as a millionth of a millimetre) and the crystal structure of these layers is perfectly aligned with that of the substrate.

B.S.KWka *et al.* [50] grown MgO film on fused silica substrate and Si(100) substrate. On fused silica substrate, they can obtain MgO(100) film when the substrate temperature was 740 ℃. While there were various orientations on Si(100) substrate. The results showed that the substrate temperature and the film thickness could affect the crystallinity of the film. Jin-Hyo Boo *et al.* [51] grew MgO film on Si(100) substrate and *c*-plane sapphire substrate. They found that the growth temperature and the substrate type or source were the important factors which affected the crystal orientation or crystallinity.

Collection @ kmou

3.2.4 Pulsed laser deposition (PLD)

Pulsed laser deposition (PLD) is a physical vapor deposition (PVD) technique where a high-power pulsed laser beam is focused inside a vacuum chamber to strike a target of the material which is to be deposited. This material is vaporized from the target (in a plasma plume) which deposits it as a thin film on a substrate (such as a silicon wafer facing the target). This process can occur in ultra-high vacuum or in the presence of a background gas, such as oxygen which is commonly used when depositing oxides to fully oxygenate the deposited films.

Generally, it has four processes:

(a) material consistent is vaporized and the plasma is generated.

(b) the thermal emission of the local oriented plasma will take place.

(c) exciton and plasma will interact with the substrate surface.

(d) the film will condensate on the substrate surface.

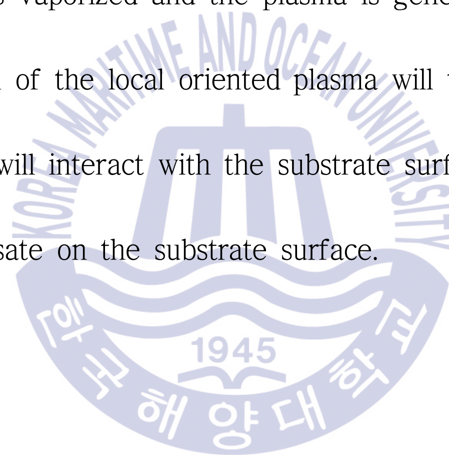

Collection @ kmou

3.4 The Analysis Methods of MgO Film

3.4.1 X-ray Diffraction (XRD)

X-ray diffraction (XRD) is a powerful nondestructive technique for characterizing crystalline materials. It provides information on structures, phases, preferred crystal orientations (texture), and other structural parameters, such as average grain size, crystallinity, strain, and crystal defects. It is based on constructive interference of monochromatic X-rays and a crystalline sample: The X-rays are generated by a cathode ray tube, filtered to produce monochromatic radiation, collimated to concentrate, and directed toward the sample. The interaction of the incident rays with the sample produces constructive interference (and a diffracted ray) when conditions satisfy Bragg's Law ($n\lambda = 2d\sin\theta$). This law relates the wavelength of electromagnetic radiation to the diffraction angle and the lattice spacing in a crystalline sample. X-ray diffraction peaks are produced by constructive interference of a monochromatic beam of x-rays scattered at specific angles from each set of lattice planes in a sample. The peak intensities are determined by the distribution of atoms within the lattice. Consequently, the X-ray diffraction pattern is the fingerprint of periodic atomic arrangements in a given material. A search of the ICDD standard database of X-ray diffraction patterns enables quick phase identification for a large variety of crystalline samples.

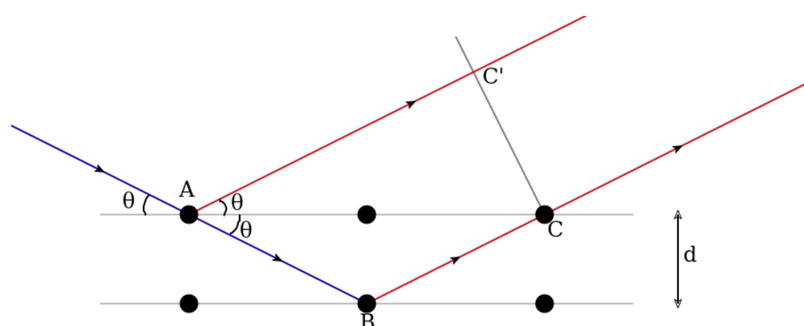

Fig. 3.7 Schematics of Bragg's law where d is the interplanar spacing and θ is diffraction angle

Bragg diffraction occurs when radiation, with wavelength comparable to atomic spacing,

Collection @ kmou

is scattered in a specular fashion by the atoms of a crystalline system, and undergoes constructive interference. Suppose that a single monochromatic wave (of any type) is incident on aligned planes of lattice points, with interplanar spacing d, at diffraction angle θ. Points A and C are located on one plane, and B is on the below plane. Points ABCC' form a quadrilateral.

There will be a path difference between the ray that gets reflected along AC' and the ray that gets transmitted, then reflected, along AB and BC respectively. This path difference is

$$(AB + BC) - (AC').$$

The two separate waves will arrive at a point with the same phase, and hence undergo constructive interference, if and only if this path difference is equal to any integer value of the wavelength, i.e.

$$(AB + BC) - (AC') = n\lambda,$$

where the same definition of n and λ applied as above.

Therefore,

$$AB = BC = \frac{d}{\sin\theta} \text{ and } AC = \frac{2d}{\tan\theta},$$

from which it follows that

$$AC' = AC \cdot \cos\theta = \frac{2d}{\tan\theta}\cos\theta = \left(\frac{2d}{\sin\theta}\cos\theta\right)\cos\theta = \frac{2d}{\sin\theta}\cos^2\theta.$$

Putting everything together,

$$n\lambda = \frac{2d}{\sin\theta}(1 - \cos^2\theta) = \frac{2d}{\sin\theta}\sin^2\theta,$$

which simplifies to

$$n\lambda = 2d\sin\theta,$$

which is Bragg's law.

If only two planes of atoms are diffracting, as shown in the pictures, then the transition

Collection @ kmou

from constructive to destructive interference would be gradual as a function of angle, with gentle maxima at the Bragg angles. However, since many atomic planes are interfering in real materials, very sharp peaks surrounded by mostly destructive interference result.

MgO belongs to NaCl cubic structure. According to formula, when the wavelength of the X-ray is determined, the diffraction peaks derived from different crystal MgO surface will correspond to a certain diffraction angle θ. In the XRD spectra, if the corresponding 2θ value of a diffraction peak is larger (eg. over 1°) than the standard value, or that there are some other diffraction peaks which don' t belong to MgO, it is possible that the material is doped with other impurities. We should take this problem seriously in this case. For the clean MgO films, the growth orientation is almost single. However, only by θ-2θ scan cannot determine whether the film is a single crystal or not. In this case, we need to scan the samples through the inner surface or double crystal X-ray diffraction to solve this problem. If the FWHM is smaller, it can also illustrate that the film crystallization is very good . In a short, if we can eliminate the influence of some factors, such as differences in film thickness, uniformity and other errors, a smooth surface and a strong peak mean that the film crystallinity is very good.

According to Scherrer equation (shown as equation 2.4) [52],we can estimate the grown size.

$$D = \frac{0.9\lambda}{B\cos\theta_B} \tag{2.4}$$

where:

D is the mean size of the ordered (crystalline) domains, which may be smaller or equal to the grain size;

K is a dimensionless shape factor, with a value close to unity. The shape factor has a typical value of about 0.9, but varies with the actual shape of the crystallite;

λ is the X-ray wavelength;

Collection @ kmou

B is the line broadening at half the maximum intensity (FWHM), after subtracting the instrumental line broadening, in radians. Sometimes this quantity is also denoted as $\Delta(2\theta)$

θ is the Bragg angle.

Generally, the smaller B is, the greater D is. So the grain size can also reflect the level of the crystalline quality of the film. But this formula only applies for the certain condition when $D <$ 100nm.

Collection @ kmou

3.4.2 Atomic Force Microscopy (AFM)

Atomic force microscopy is arguably the most versatile and powerful microscopy technology for studying samples at nanoscale. It is versatile because an atomic force microscope can not only image in three-dimensional topography, but it also provides various types of surface measurements to the needs of scientists and engineers. It is powerful because AFM can generate images at atomic resolution with angstrom scale resolution height information, with minimum sample preparation.

AFM uses a cantilever with a very sharp tip to scan over a sample surface. As the tip approaches the surface, the close-range, attractive force between the surface and the tip cause the cantilever to deflect towards the surface. However, as the cantilever is brought even closer to the surface, such that the tip makes contact with it, increasingly repulsive force takes over and causes the cantilever to deflect away from the surface.

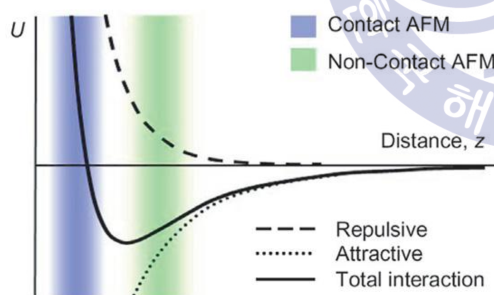

Fig. 3.8 Inter-atomic Force vs. distance

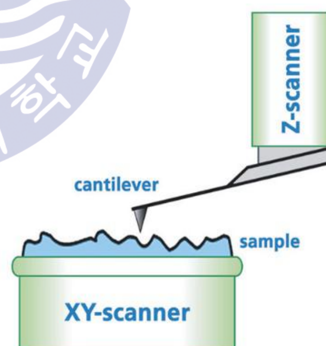

Fig. 3.9 AFM scan system

Collection @ kmou

3.4.3 Scanning Electron Microscope (SEM)

The scanning electron microscope (SEM) uses a focused beam of high-energy electrons to generate a variety of signals at the surface of solid specimens. The signals that derive from electron-sample interactions reveal information about the sample including external morphology (texture), chemical composition, and crystalline structure and orientation of materials making up the sample. In most applications, data are collected over a selected area of the surface of the sample, and a 2-dimensional image is generated that displays spatial variations in these properties. Areas ranging from approximately 1 cm to 5 microns in width can be imaged in a scanning mode using conventional SEM techniques (magnification ranging from 20X to approximately 30,000X, spatial resolution of 50 to 100 nm). The SEM is also capable of performing analyses of selected point locations on the sample. This approach is especially useful in qualitatively or semi-quantitatively determining chemical compositions (using EDS), crystalline structure, and crystal orientations (using EBSD). The design and function of the SEM is very similar to the EPMA and considerable overlap in capabilities exists between the two instruments.

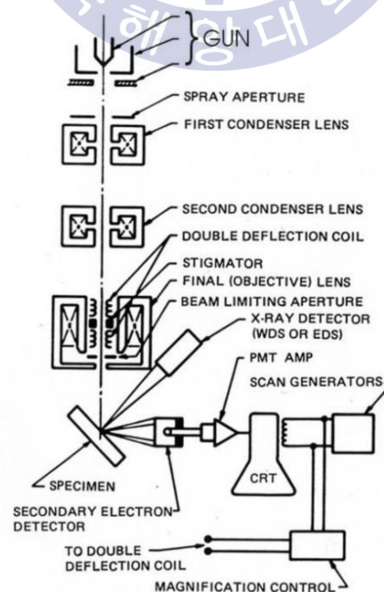

Fig. 3.10 Schematic of the electron and x-ray optics of a combined SEM-EPMA

Collection @ kmou

3.4.4 Energy-dispersive X-ray Spectroscopy (EDX)

Energy-dispersive X-ray spectroscopy (EDS, EDX, or XEDS), is an analytical technique used for the elemental analysis or chemical characterization of a sample. It relies on an interaction of some source of X-ray excitation and a sample. Its characterization capabilities are due in large part to the fundamental principle that each element has a unique atomic structure allowing unique set of peaks on its X-ray emission spectrum. To stimulate the emission of characteristic X-rays from a specimen, a high-energy beam of charged particles such as electrons or protons (see PIXE), or a beam of X-rays, is focused into the sample being studied. At rest, an atom within the sample contains ground state (or unexcited) electrons in discrete energy levels or electron shells bound to the nucleus. The incident beam may excite an electron in an inner shell, ejecting it from the shell while creating an electron hole where the electron was. An electron from an outer, higher-energy shell then fills the hole, and the difference in energy between the higher-energy shell and the lower energy shell may be released in the form of an X-ray. The number and energy of the X-rays emitted from a specimen can be measured by an energy-dispersive spectrometer. As the energies of the X-rays are characteristic of the difference in energy between the two shells and of the atomic structure of the emitting element, EDS allows the elemental composition of the specimen to be measured.

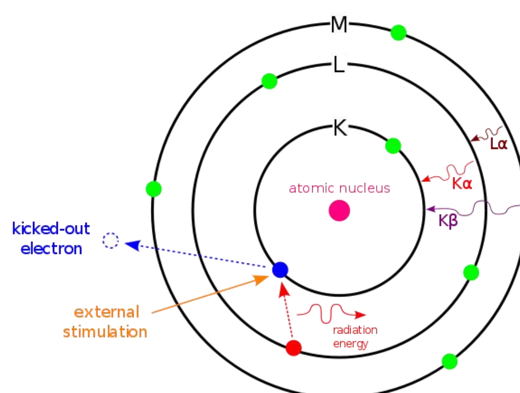

Fig. 3.11 Principle of EDS measurement

Collection @ kmou

3.4.5 Transmission Electron Microscopy(TEM)

Transmission electron microscopy (TEM) is a microscopy technique in which a beam of electrons is transmitted through an ultra-thin specimen, interacting with the specimen as it passes through it. An image is formed from the interaction of the electrons transmitted through the specimen; the image is magnified and focused onto an imaging device, such as a fluorescent screen, on a layer of photographic film, or to be detected by a sensor such as a CCD camera.

TEMs are capable of imaging at a significantly higher resolution than light microscopes, owing to the small de Broglie wavelength of electrons. This enables the instrument's user to examine fine detail—even as small as a single column of atoms, which is thousands of times smaller than the smallest resolvable object in a light microscope. TEM forms a major analysis method in a range of scientific fields, in physical, chemical and biological sciences. TEMs find application in cancer research, virology, materials science as well as pollution, nanotechnology, and semiconductor research.

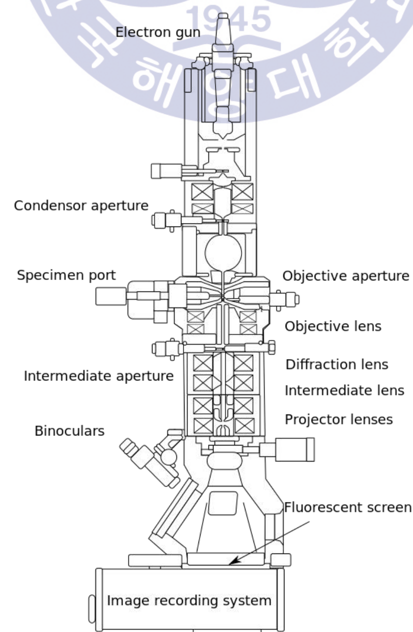

Fig. 3.12 Layout of optical components in a basic TEM

Collection @ kmou

Chapter 4. Results and Discussions

4.1 Experiment and Procedure

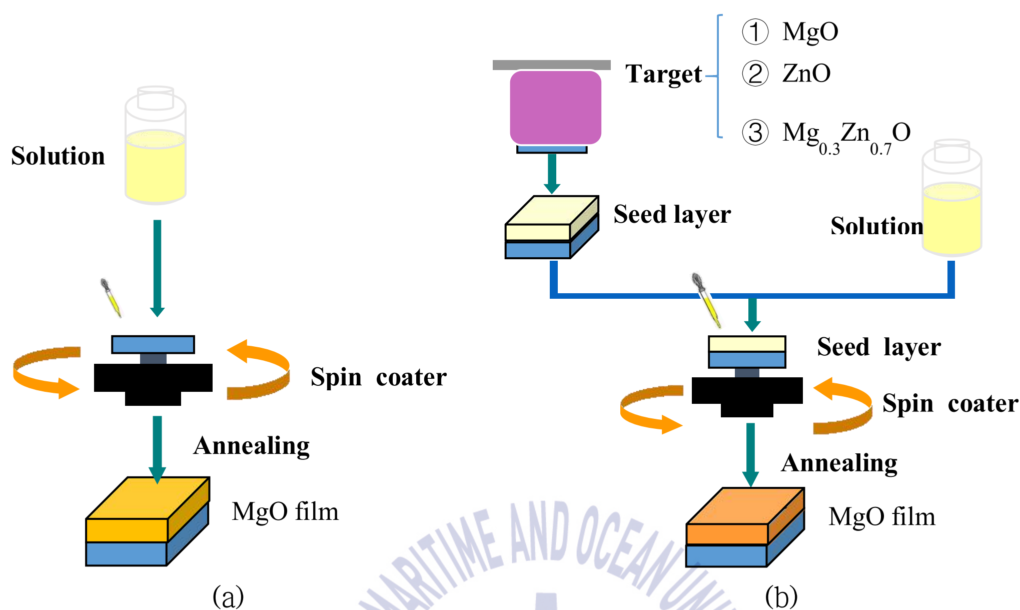

Fig. 4.1 Basic procedure of the experiment. (a) presents the comparison which has no buffer layer compared with (b)

The precursor solution of MgO, about 0.2M concentration, was prepared by dissolving magnesium ethoxide in 2-methoxyethanol [53,54]. A patially-hydrolysed precursor was filtered to remove the undissolved substance and the large particles.

Table 4.1 The parameters of the solution

Parameter	Value
Material	Magnesium ethoxide, 2-methoxyethanol Concentration
Concentration	0.2 M
Stir speed	600 rpm
Stir time	2 h
Temperature	room temperature

The Si(100) substrates (1cm × 1cm) were etched with diluted HF (10%) for 2 min followed by ultrasonic cleaning in aceton and ethanol for 10 min, respectively. After that, the Si substrate were rinsed with deionized water for 10 min under ultrasonic conditions and

Collection @ kmou

then blow-dried by N_2 gun. The MgO buffer layer was deposited on Si substrate by RF magnetron sputtering operating under different conditions as shown in Table 4.1. During the growing process, the substrate temperature was maintained at 300℃ in the chamber. The chamber was first evacuated to a base pressure of $\approx 1\times10^{-6}$ Torr, and then Ar was introduced at a total working pressure of 5 mTorr. The total working pressure was kept constant during the deposition.

After that the precursor was deposited on the Si substrates which possessed a different buffer layer deposited by RF sputtering process. The MgO films consisting of 8 layers were prepared by spin coating at 3000 rpm for 25s. After every two layers deposited, the coated substrates were heated up to 350 ℃ in air with a ramping rate of 5℃/s in rapid thermal annealing (RTA) chamber and then cooled down. After spin coating, heat-treatment was conducted at 700℃, 800℃ and 900℃ for 1h in oxgen to achieve the oxidization of magnesium. For comparison, another set of experiments were performed using the Si(100) substrate without RF magnetron sputtering process or without filter. The basic procedure was shown as Fig. 4.1.

KOREA MARITIME AND OCEAN UNIVERSITY 1945 한국해양대학교

Table 4.2 The main condition parameters of the experiment

<table>
<tr><th colspan="2">Buffer layer / Condition</th><th>None</th><th>MgO</th><th>ZnO</th><th>$Mg_{0.3}Zn_{0.7}O$</th><th></th></tr>
<tr><td rowspan="4">RF Sputtering</td><td>power</td><td></td><td>300 W</td><td>100 W</td><td>300 W</td><td></td></tr>
<tr><td>temperature</td><td></td><td colspan="3">300 ℃</td><td></td></tr>
<tr><td rowspan="2">time</td><td></td><td>30 min</td><td>10 min</td><td>30 min</td><td>①</td></tr>
<tr><td></td><td>1 h</td><td>30 min</td><td>30 min</td><td>②</td></tr>
<tr><td rowspan="4">Spin coating</td><td>speed</td><td colspan="4">3000 rpm</td><td rowspan="4"></td></tr>
<tr><td>time</td><td colspan="4">25 s</td></tr>
<tr><td>times</td><td colspan="4">8</td></tr>
<tr><td>temperature</td><td colspan="4">room temperature</td></tr>
<tr><td rowspan="2">Annealing</td><td>time</td><td colspan="4">1 h</td><td rowspan="2"></td></tr>
<tr><td>temperature</td><td colspan="4">700℃,800℃,900℃</td></tr>
</table>

The phase structure of the films was examined by X-Ray diffraction (XRD) using the

dCollection @ kmou

Cu K α radiation. The surface morphology of the films was investigated with atomic force microscopy (AFM). Scanning electron microscope (SEM) and transmission electron microscope(TEM) were used to investigated the microstructure of the surface and cross section. The compositional fluctuation of the surface was also examined by energy-dispersive X-ray spectroscopy (EDAX).

Collection @ kmou

4.2 The Characteristics of the MgO Film Grown on Si(100) Substrate

4.2.1 The Analysis of XRD

Fig. 4.2 was the XRD profile of the samples which were processed under different conditions. In order to make a clear comparison, we also grow the MgO film on Si(100) substrate without buffer layer as shown as Fig. 4.1(a). According to Fig. 4.2 , we successfully obtained the (111)-oriented MgO film. Based on the buffer layer, MgO(111) orientation peaks easily occurred from 700℃. Jong-Gul Yoon *et al.* obtained MgO(111) film on Si(111) and Si(100) substrate [4]. They also pointed that (111) orientation was independent with the substrate orientation. Furthermore, it was easier to obtain MgO(111) film on Si(111) substrate than that on Si(100) substrate.

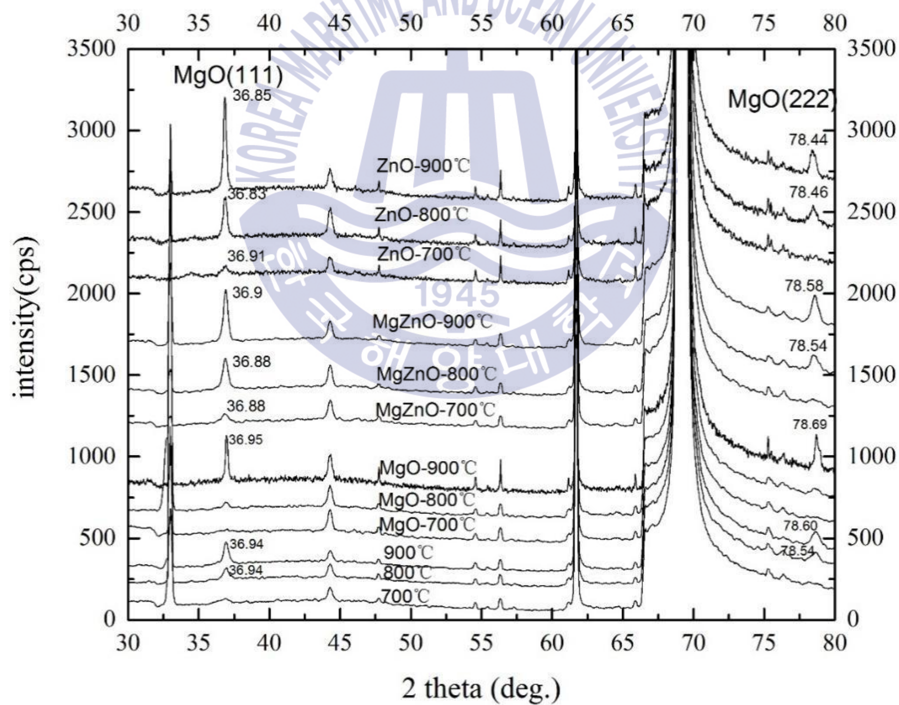

Fig. 4.2 XRD profile of the samples which had different buffer layer annealed at various temperature

Jong-Gul Yoon *et al.* discussed the factors which could affect the crystallization direction of MgO film [54]. The surface structure of the semiconductor before deposition was the first factor. The second was SiO_2 inter-layer which formed during the deposition. They believed that the SiO_2 inter-layer was difficult to avoid to be formed. There were two

Collection @ kmou

stages for SiO_2 inter-layer to form. Pyrolysis process was the first stage and the second stage was crystallization process during which the oxygen molecule could diffuse deeply so that a chemical reaction with the substrate could take place to form the SiO_2 inter-layer. As for this experiments, a mixed solution HF:H_2O(1:10) was used to etch the oxide on the substrate and introduced buffer layer. That could reduce the influence of SiO_2 inter-layer which were mentioned by Jong-Gul Yoon [54].

Cao Xiao-yan *et al.* mentioned that someone successfully obtained unidirectionally oriented MgO(110), MgO(100) and MgO(111) by MBE method and they found that the orientation of the film was only affected by the substrate temperature [55]. The orientation had no relation with pressure, pulsed laser speed and etching the substrate. They also pointed out the mechanism of preparing MgO film by using sol-gel method. Mg atom combined the O atom in the air and they would crystallize at high temperature. (111) orientation was strictly according to the mode that one O atom layer and one Mg atom layer overlay together to grow. So the condition was modified to make the thickness of ZnO buffer layer much thicker. To achieve this goal, sputtering time was extended from 10 min to 30 min. The XRD result was shown as Fig. 4.3. As for ZnO buffer layer, only (002) orientation occurred. But MgO(111) could be also obtained on ZnO(002) buffer layer.

Collection @ kmou

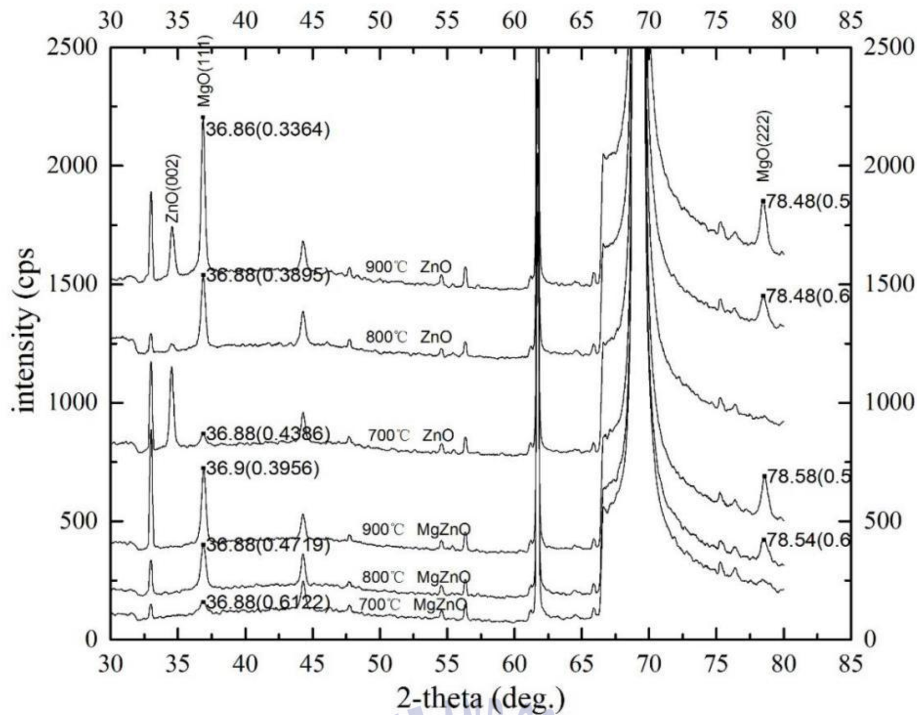

Fig. 4.3 XRD profile of samples which were sputtered for 30 mins

It's found that the orientation of the prepared MgO film has no relation with that of the substrate. (111) orientation was much easier to occur. That maybe because that the {111} crystal orientation has a higher growth rate [54]. The orientation of the substrate and the inter-layer only affect the difficulty and the intensity of a certain crystal orientation that the film could form.

On the whole, (111) orientation was much more preferred according XRD results. Fig. 4.4 showed the relation between FWHM and annealing temperature. Under a certain degree, the intensity of (111) and (222) orientation increased and FWHM of that became smaller with temperature increased. That means that the crystal quality became better with the annealing temperature increased. According to the theory of nucleation, in the not very high temperature range, as the substrate temperature increasing, the ion source which are adsorbed on the substrate surface will get more thermal energy. That will accelerate the surface mobility which will make a contribution to their migration to the thermodynamic equilibrium position. So the crystalline quality of the film should be improved with the annealing temperature increased. However, once the temperature

Collection @ kmou

exceeds this certain high extent, the source of particles dominates the adsorption process so that the crystal profile of the film deteriorates.

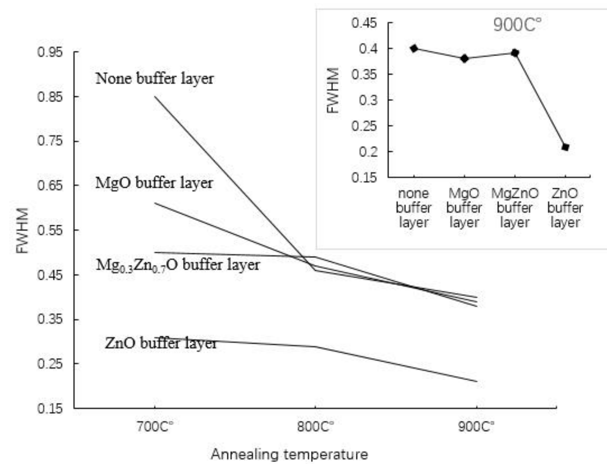

Fig. 4.4 FWHM profile of the samples which were annealed at different temperature

In theory, MgO buffer layer should work best. But compared those three buffer layer, ZnO buffer layer generated the best result. Fig. 4.5 showed the epitaxy relationship between cubic MgO(111) and hexagonal ZnO(0001). Due to the similar structural property, ZnO buffer layer can reduce the lattice mismatch to a large extent between MgO thin film and Si(100) substrate. Besides, the crystal quality of MgO buffer layer was not good enough. That may also account for why ZnO buffer layer worked better than MgO buffer layer.

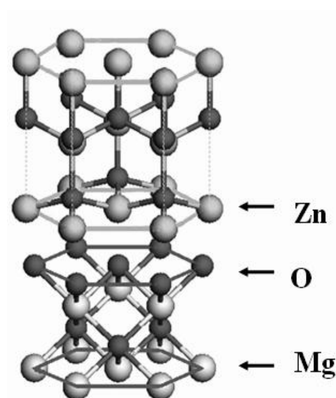

Fig. 4.5 The epitaxy relationship between cubic MgO(111) and hexagonal ZnO(0001)

Collection @ kmou

In some paper, the formation of SiO_2 during the heat-treatment was mentioned [4,54]. The authors also discussed that the SiO_2 could effect the preferred orientation of MgO film and caused MgO(111) peak occurred on Si(100) substrate. But the existence of ZnO buffer layer could reduce the effect of SiO_2. The (111) growth orientation of MgO films prepared by sol-gel method may be due to the higher growth rate for the {111} faces as well. From this aspect, it seemed that the independence of preferred orientation between MgO film and Si substrate was also due to the material we used in our experiment. As for $Mg_{0.3}Zn_{0.7}O$ buffer layer, due to the doping of Mg atom, the roughness of the buffer layer surface may be relatively larger than that of ZnO buffer layer. That prevented the diffusion of Mg atom on $Mg_{0.3}Zn_{0.7}O$ buffer layer interface to some extent. It resulted in a big clusters and blurred rough uneven surface of the film [56]. That may affect the crystallization of the MgO film. As for MgO buffer layer which was deposited on substrate for 1 h, the improvements were not obviously when the temperature under 900℃. That maybe because of the bad carystal quality of buffer layer.

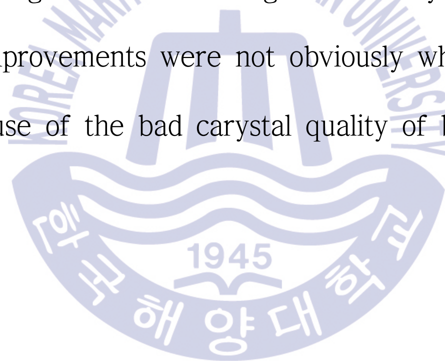

Collection @ kmou

4.2.2 The Analysis of AFM

The surface topography of the samples was observed, as shown in Fig. 4.6 and Fig. 4.7. From the AFM results, the film which had big clusters and blurred rough uneven surface could be obtained when the annealing temperature was not high. It was probably due to low temperatures, the atoms on the Si substrate did not absorb enough energy to diffuse and the weak interaction during crystallization process resulted in an unconspicuous crystallization [56]. Under certain extent, the increase of the annealing temperature accelerated the growth of the film. The particles became uniform and the boundary became much clear. MgO particles arranged orderly and the surface defects were reduced so that the MgO film became much smooth. The surface roughness was reduced and the grain size increased. The grain size became larger as well. That indicated that the quality of the film was getting better. According to Fig. 4.7, pyramidal columnar morphology growth structure could be observed. With the temperature increasing, the pyramidal morphology was developed and the surface become smoother and exhibited a low surface roughness. But after annealed at above 800℃, Fig. 4.6(b) showed a smaller roughness compared with Fig. 4.6(a).

Collection @ kmou

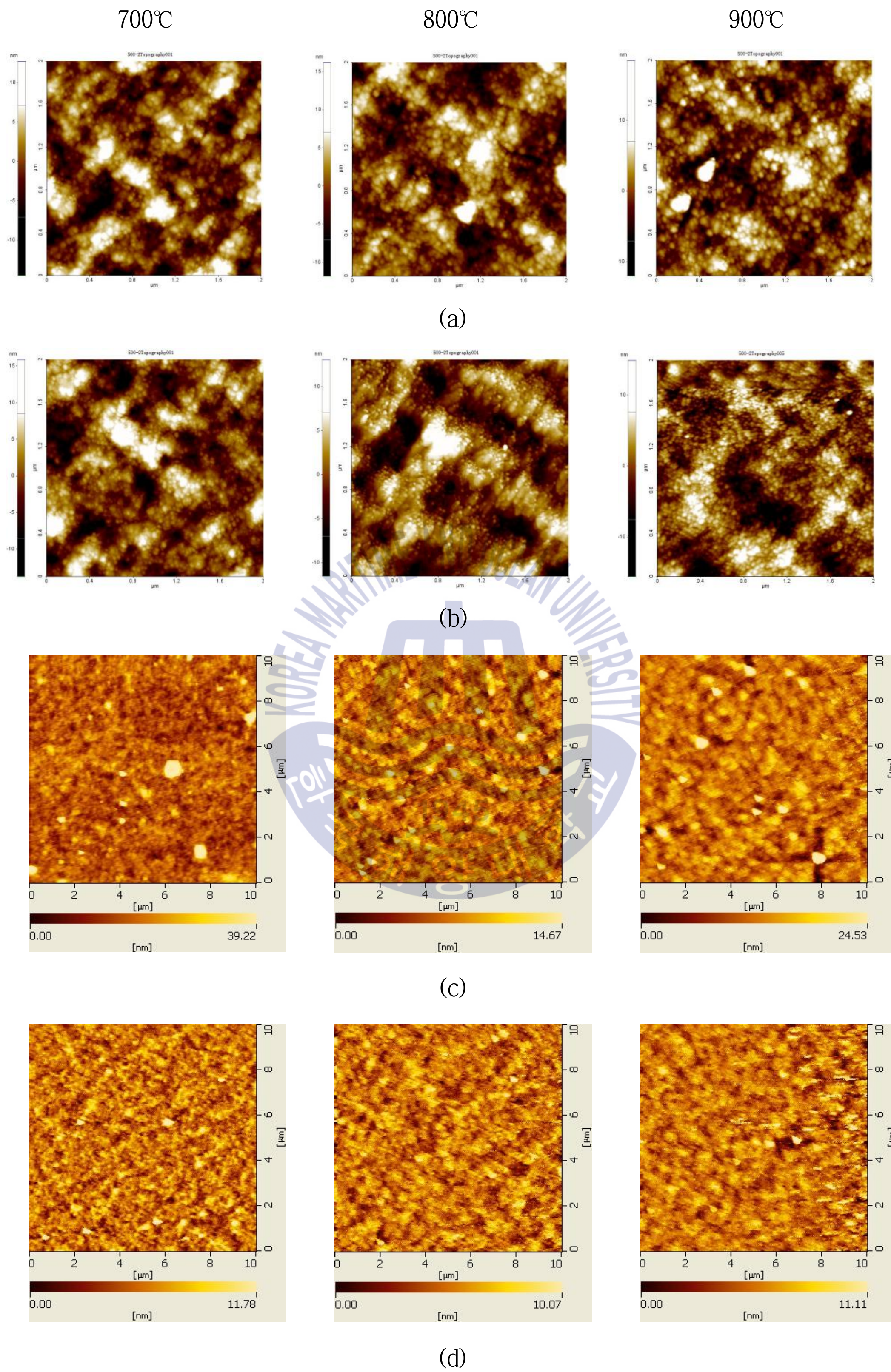

Fig. 4.6 AFM results of the MgO films which were grown on (b) MgO buffer layer, (c) ZnO buffer layer and (d) $Mg_{0.3}Zn_{0.7}O$ buffer layer

Collection @ kmou

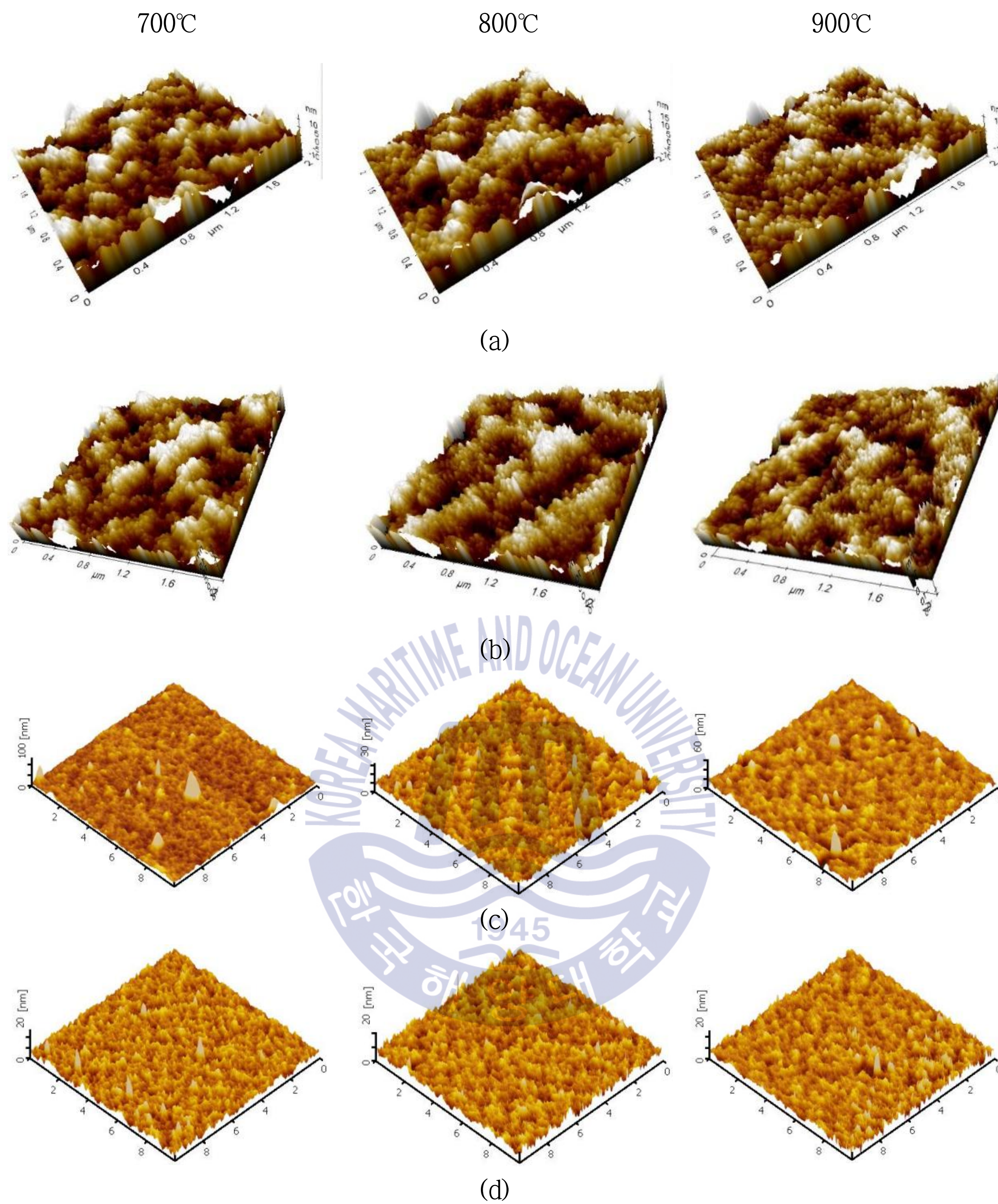

Fig. 4.7 3D morphology of MgO thin films which were grown on (b) MgO buffer layer, (c) ZnO buffer layer and (d) $Mg_{0.3}Zn_{0.7}O$ buffer layer

According Fig. 4.8, with the temperature increasing, totally the grain size became larger and the RMS changed oppositely. After 900℃ annealed, the uniform size distribution could be found in Fig. 4.6. The particle became more rounded. But aggregation of MgO particle at the surface could also be found in the Fig. 4.6. That maybe resulted a larger RMS inordinately. After introducing ZnO buffer layer and $Mg_{0.3}Zn_{0.7}O$ buffer, the grain size

Collection @ kmou

was larger than that using MgO buffer layer. But ZnO buffer layer effected it strongly. Compared with ZnO buffer layer, the roughness of MgZnO buffer layer was larger due to the doping of Mg atoms. It hindered the movement of the atoms on the buffer layer to some extent.

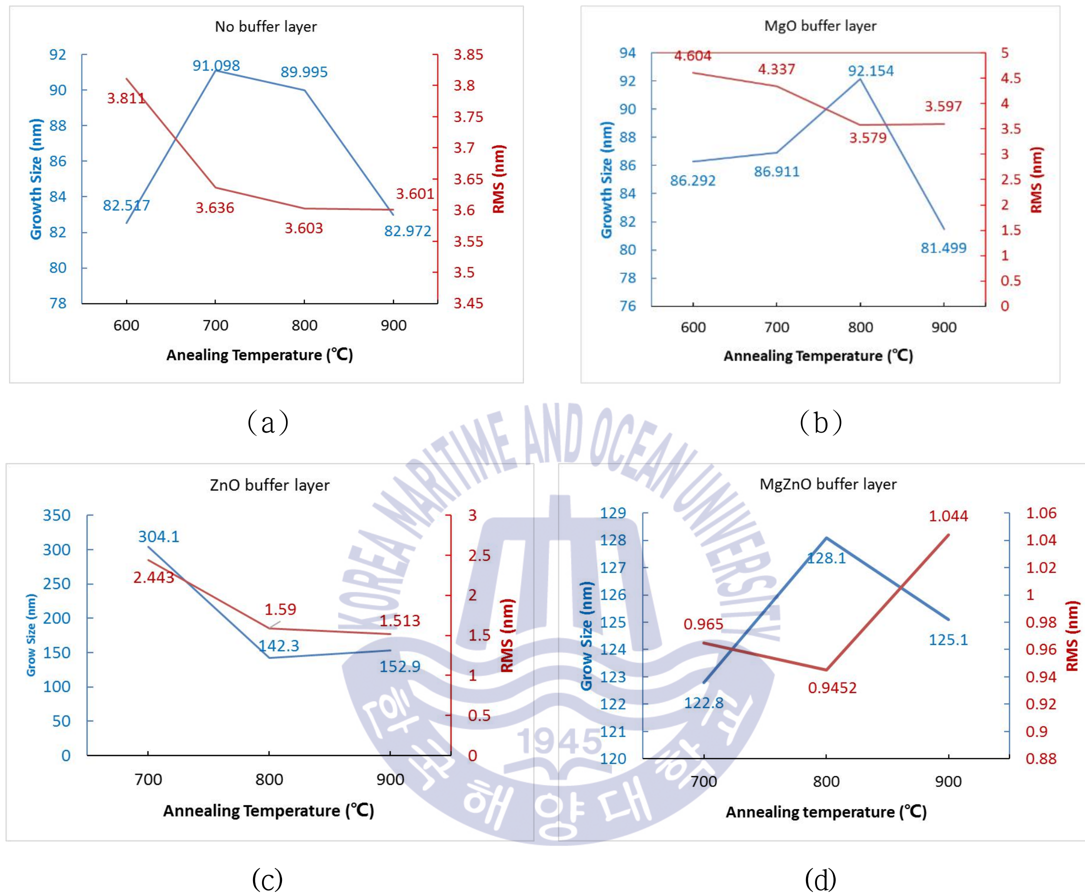

(a) (b)

(c) (d)

Fig. 4.8 The relation between grain size and RMS

In short, as the annealing temperature increasing, the atoms within the crystals became much more active. Around the crystal boundary, the dangling bonds combined with each other and formed a relatively metastable bond. That make the crystal grow and reduced the interface state. As a result, the film crystalline quality was improved. It was mainly two-dimensional growth mode during this process. While the annealing temperature was further increased, the atoms on the surface absorbed the excess energy and then gathered into a three-dimensional cluster of particles [56].

Collection @ kmou

4.2.3 The Analysis of SEM and TEM

According to Fig. 4.9, the surface showed a porous or cracked surface microstructure even though the drying and heating process have been optimized. Fig. 4.9(a) and (b) were the result of the samples which the solution was spin coated on after filter process. Fig. 4.9(c) was the result that the solution was not filtered. It was found that the surface in Fig. 4.9(c) had serious cracks and a lot of clusters which had different sizes occurred on the surface. Maybe It was because that there were some slightly soluble or insoluble particles in the prepared solution, such as $Mg(OH)_2$, which were very easy to be formed [57]. During the spin coating process, these large particles seriously affected the uniform distribution of the solution on the substrate surface. The surface roughness was extremely enlarged, as well as difficult of forming a uniform film. During post-annealing process, due to the different thermal expansion coefficient of each region, crack was taken place as shown in Fig. 4.9(c).

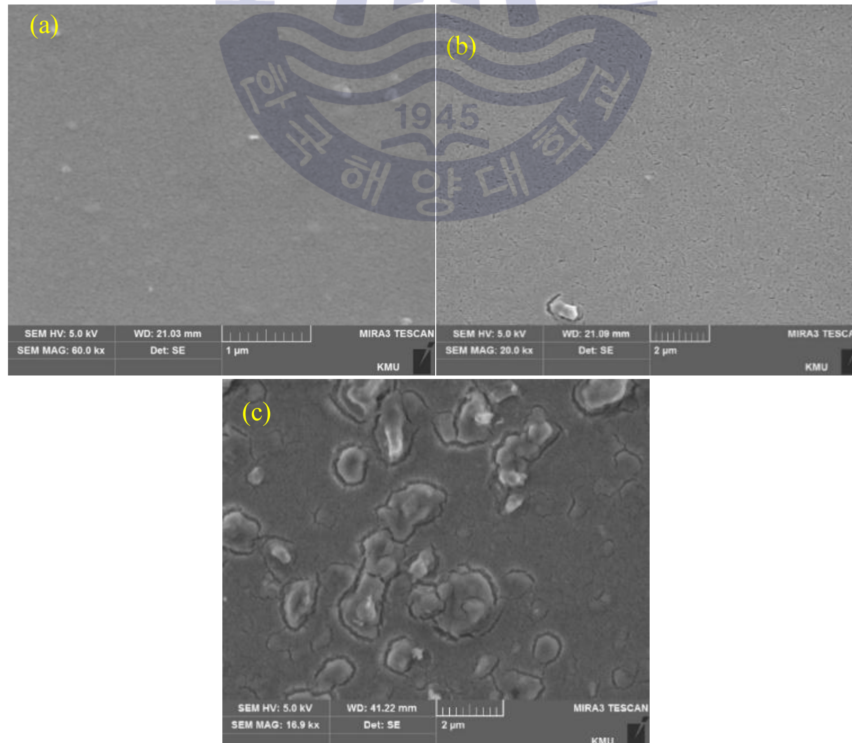

Fig. 4.9 Surface morphology of the samples observed by SEM after annealed at 900℃. The sample (a) and (b) were processed under condition ② as shown in Table 3.2; samples (c) was processed without filter process

Collection @ kmou

These cracks may also lead to instability in electron emission from the surface and furthermore, reduce the lifetime of PDP because the dielectric layers cannot be effectively protected during long time operation [61]. So the MgO film shown in Fig. 4.9(c) cannot be used as the substrate film in some applications.

Fig. 4.10 showed the samples which were processed with filter. It was found that the surface of the samples became smooth after introducing buffer layer. The cracking phenomenon has been effectively reduced effectively.

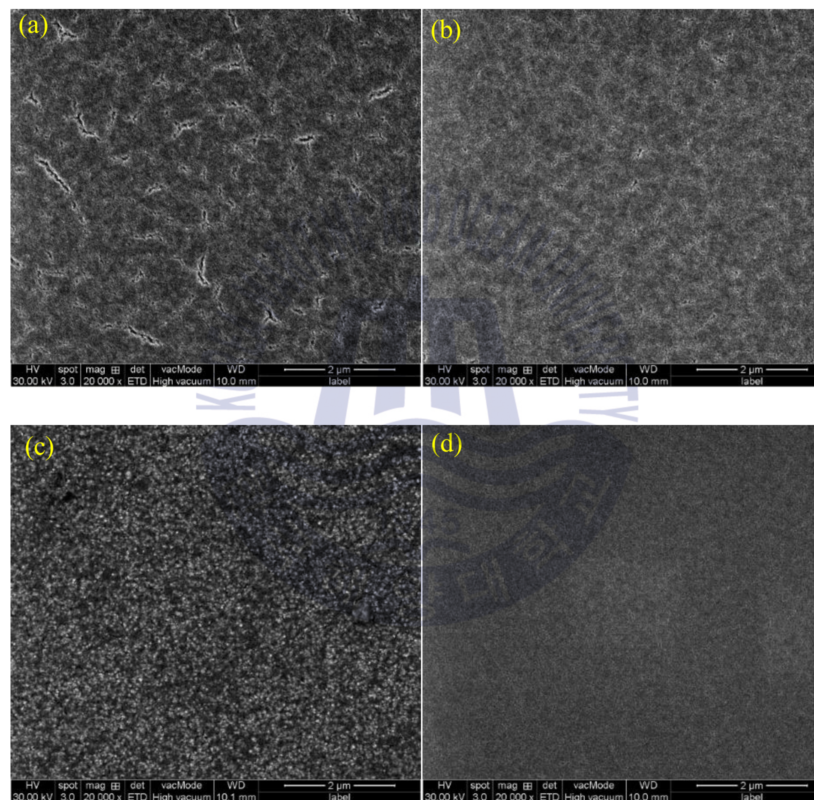

Fig. 4.10 The surface of the samples obtained by TEM

According to Fig. 4.11, the cross section showed a dense microstructure and the film was uniform. The thickness was around 156 nm which was coated 8 times and the boundary between MgO film and the Si substrate was clear. As for those three buffer layer, due to the high growth rate, the thickness of ZnO buffer layer was largest. In addition, the caystal quality of ZnO buffer layer was very good. That may accout for why ZnO buffer layer worked better than the other two buffer layers.

Collection @ kmou

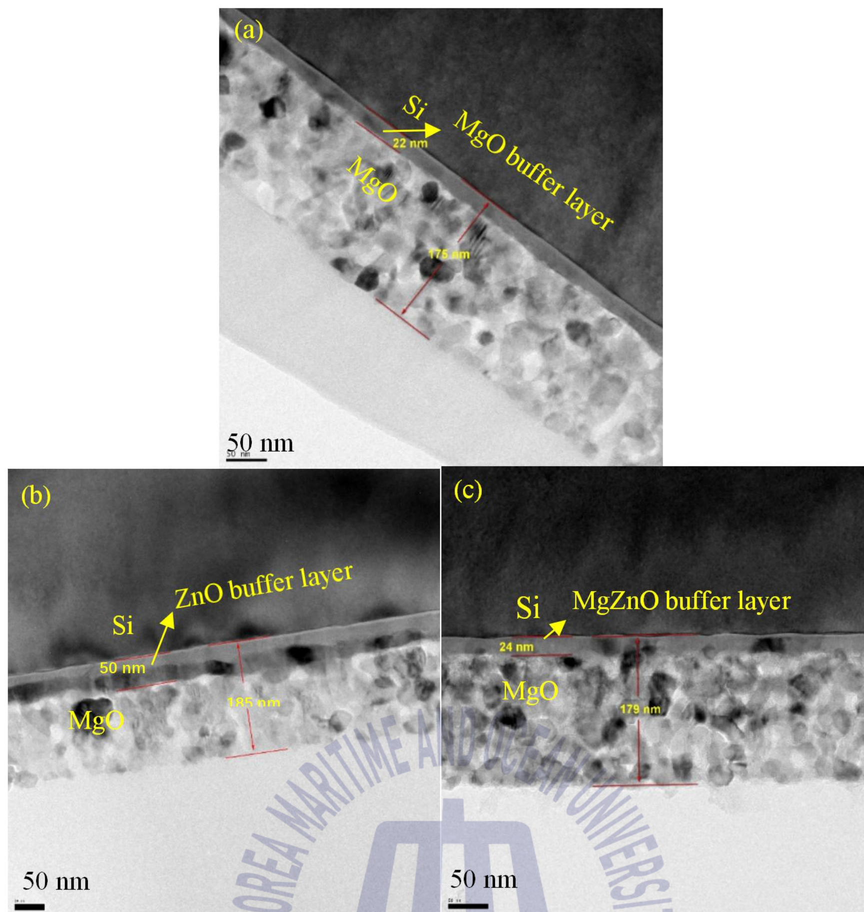

Fig. 4.11 The cross section of the samples which were based on (a) MgO buffer layer, (b) ZnO buffer layer and (c) Mg0.3Zn0.7O buffer layer

Collection @ kmou

Chapter 5. Summary and Conclusion

This experiment aimed to grow MgO film on Si(100) substrate by combining RF magnetron sputtering and sol-gel method. XRD, SEM, AFM and TEM were used to investigate the properties of the films. The effects of the buffer layer and the temperature were also analyzed and the final analysis conclusions were summarized as the following items:

(1) In this experiment, (111) was the preferred orientation, which due to the higher growing rate of {111}.

(2) Buffer layer could reduce the degree of difficulty to prepare MgO film and improve the quality of the MgO film. Based on the buffer layer, MgO(111) peaks easily occurred from 700℃.

(3) At a given substrate temperature, ZnO buffer layer worked best. That maybe due to the similar structure between MgO(111) and ZnO(0001) and the good crystal quality . MgZnO could improve the quality of MgO film as well. But due to the doping of Mg atom, the surface roughness of MgZnO was larger than that of ZnO. That effected the movement of MgO molecule on the surface. Due to the thickness of MgO buffer layer was too thin or the bad crystal quality, it cannot reduce the lattice mismatch significantly so that the MgO buffer layer had no evident effect on the improvement of MgO film.

(4) The substrate temperature could improve the crystal quality of MgO film. In general, increasing annealing temperature could improve the crystal quality of the film. But the substrate temperature had no effect on the formation of the preferred orientation.

Although we can obtain MgO film which has better structural properties on Si(100) by the method mentioned in this paper, the optical and electrical properties of the films are still not investigated. Thus, the next work will focus on those properties to make sure the availability of the method we used.

Collection @ kmou

Reference

[1] Z.P. Li, X. Guo, H.B. Lu, Z.L. Zhang, *et al.*, Advanced Materials, 26(42), (2014), 7185-7189.

[2] J.H. Kim, S.I. Khartsev & A.M. Grishin, Appl. Phys. Lett., 82, (2003), 4295.

[3] B. Vilquin, G. Niu, S. Yin, A. Borowiak, *et al.*, In Access Spaces (ISAS), 2011 1st International Symposium on. IEEE, (2011), 294-298.

[4] J.G. Yoon & K. Kim, Appl. Phys. Lett., 66, (1995), 2661.

[5] J.M. Phillips, J. Appl. Phys., 79, (1996), 1829.

[6] X. Gao, D. Fang, X. Fang, J. Tang, *et al.*, Materials Research Express, 2(9), (2015), 095902.

[7] W.J. DeSisto & R.L. Henry, Appl. Phys. Lett., 56, (1990), 2522.

[8] J.G. Lisoni, M. Siegert, C.H. Lei, W. Biegel, *et al.*, Thin Solid Films, 389, (2001), 219-226.

[9] B. Mazumder, V. Purohit, M. Gruber, A. Vella, *et al.*, Thin Solid Films, 589, (2015), 38-46.

[10] D. Velázquez, R. Seibert, Z. Yusof, J. Terry, *et al.*, International Particle Accelerator Conference, Richmond, VA, USA. 2015.

[11] J. Wollschläger, J. Viernow, C. Tegenkamp, D. Erdös, *et al.*, Applied Surface Science, 142, (1999), 129-134.

[12] M.C. Gallagher, M.S. Fyfield, L.A. Bumm, J.P. Cowin, *et al.*, Thin Solid Films, 445, (2003), 90-95.

[13] H. Kupfer, R. Kleinhempel, F. Richter, C. Peters, *et al.*, Journal of Vacuum Science & Technology A, 24(1), (2006), 106-113.

[14] V.V. Afanas'ev, A. Stesmans, K. Cherkaoui & P.K. Hurley, Appl. Phys. Lett., 96, (2010), 052103.

[15] S.W. Kang, Y.Y. Kim, C.H. Ahn, S.K. Mohanta, *et al.*, Journal of Materials Science: Materials in Electronics, 19(8-9), (2008), 755-759.

[16] Ü. Özgür, Y.I. Alivov, C. Liu, A. Teke, *et al.*, J. Appl. Phys., 98, (2005), 041301.

Collection @ kmou

[17] T. Hanada, Oxide and Nitride Semiconductors, Springer Berlin Heidelberg, 12, (2009), 1-19.

[18] Y. Liu, Q.Y. Hou, H.P. Xu, L.M. Li, *et al.*, Physica B, 407, (2012), 2359-2364.

[19] D.K. Hwang, M.C. Jeong & J.M. Myoung, Applied surface science, 225(1), (2004),: 217-222.

[20] D.C. Look, B. Claflin, Ya.I. Alivov & S.J. Park, physica status solidi (a), 201(10), (2004), 2203-2212.

[21] D.K. Hwang, S.H. Kang, J.H. Lim, E.J. Yang, *et al.*, Appl. Phys. Lett., 86(22), (2005), 222101-222101.

[22] Agnieszka Kołodziejczak-Radzimska & Teofil Jesionowski, Materials, 7(4), (2014), 2833-2881.

[23] Y.N. Hou, Z.X. Mei, H.L. Liang, D.Q. Ye, *et al.*, Appl. Phys. Lett., 102(15), (2013), 153510.

[24] W.Z. Liu, H.Y. Xu, J.G. Ma, C.Y. Liu, Appl. Phys. Lett., 100(20), (2012), 203101.

[25] L.K. Wang, Z.G. Ju, J.Y. Zhang, J. Zheng, *et al.*, Appl. Phys. Lett., 95(13), (2009), 131113.

[26] X. Chen & J. Kang, Semiconductor Science and Technology, 23(2), (2008), 025008.

[27] E.M. Levin, C.R. Robbins & H.F. McMurdie, M.K. Reser American Ceramic Society, Columbus, Ohio, 7, (1964).

[28] A. Ohtomo, M. Kawasaki, T. Koida, K. Masubuchi, *et al.*, Appl. Phys. Lett., 72(19), (1998), 2466-2468.

[29] I. Takeuchi, W. Yang, K.S. Chang, M. A. Aronova, *et al.*, J. Appl. Phys., 94(11), (2003), 7336-7340.

[30] L.K. Wang, Z.G. Ju, C.X. Shan, J. Zheng, *et al.*, Journal of Crystal Growth, 312(7), (2010), 875-877.

[31] V. Sukauskas, Characterization of MgZnO epitaxial layers with high Mg concentration, (2011).

[32] Ü. Özgür, Ya.I. Alivov, C. Liu, A. Teke, *et al.*, J. Appl. Phys., 98, (2005), 041301.

Collection @ kmou

[33] L.J. Brillson & Y. Lu, J. Appl. Phys., 109(12), (2011), 121301.

[34] K. Liu, M. Sakurai & M Aono, Sensors, 10(9), (2010), 8604-8634.

[35] D.C. Look, D.C. Reynolds, J.W. Hemsky, R.L. Jones, *et al.*, Appl. Phys. Lett., 75(6), (1999), 811-813.

[36] C. Jagadish & Stephen J. Pearton, Zinc oxide bulk, thin films and nanostructures: processing, properties, and applications, (2006), 1rd Ed. pp.17.

[37] K. Hirose, H. Nohira, K. Azuma & T. Hattori, Progress in Surface Science, 82(1), (2007), 3-54.

[38] Justin Kirschbrown, November 2007, RF/DC Magnetron Sputtering [Online] Avaliable at http://documents.tips/documents/rfdc-sputtering.html

[39] J.H Lee, J.H. Eun, S.Y. Park, S.G. Kim, *et al.*, Thin Solid Films, 435(1), (2003), 95-101.

[40] R. Soto, S. Mergui, P.E. Schmidt, Thin Solid Films, 308, (1997), 611-614.

[41] K.H. Nam, M.J. Jung, J.G. Han, T.Kopte, *et al.*, Vacuum, 75(1), (2004), 1-6.

[42] Q.J Bu, Secondary Electron Emission Charaeteristies and Thin Film Preparation Technology of MgO, M.D., Changchun University of Science and Technology, (2010).

[43] P. Li, Z.L. Lin, X.J. Wang, Q.Y. Zhao, *et al.*, Chinese Journal of Electron Devices, 34(6), (2011), 633-636.

[44] J.S. Lee, B.G. Ryu, H.J. Kwon, Y.W. Jeong, *et al.*, Thin Solid Films, 354(1), (1999), 82-86.

[45] T.W. Kim & Y.S. You, Materials Research Bulletin, 36(3), (2001), 747-754.

[46] T.W. Kim & Y.S. You, Applied Surface Science, 180(1), (2001), 162-167.

[47] A. Sugawara & K. Mae, Surface Science, 558(1), (2004), 211-217.

[48] W.S. Knodle & R. Chow, Handbook of Thin Film Deposition Processes and Techniques, Chapter 10. Molecular Beam Epitaxy, William Andrew Publication, (2001), page.383.

[49] A. Setiwan, H.J. Ko, S.K. Hong, Y. Chen, *et al.*, Thin Solid Films, 445(2), (2003), 213-218.

[50] B.S. Kwak, E.P. Boyd, K. Zhang, A. Erbil, *et al.*, Appl. Phys. Lett., 54(25), (1989). 2542-2544.

Collection @ kmou

[51] J.H. Boo, S.B. Lee, K.S. Yu, W. Koh, *et al.*, Thin Solid Films, 341(1), (1999), 63-67.

[52] B.D. Cullity & S.R. Stock, Elements Of X-Ray Diffraction Addison-Wesley Series in Metallurgy And Materials, (1978), 102.

[53] S. Fujihara, C. Sasaki & T. Kimura, Journal of the European Ceramic Society, 21(10), (2001), 2109-2112.

[54] J.G. Yoon & H.K. Kim, Journal of the Korean Physical Society, 31, (1997), 613-616.

[55] X.Y. Cao & H. Ye, Journal of Zhejiang University (Engineering Science), 39(4), (2005), 461-464.

[56] J.D. Zhang & L.X. Che, Journal of Baicheng Normal University, 5, (2011), 1-4.

[57] A. Kumar & J. Kumar, 2006, In: New Delhi, On the Preparation and Characteristics of Hydration Free Magnesium Oxide Films for Plasma Display Panels, The 9th Asian Symposium on Information Display, pp.380-383.

[58] W.J. Fu, X.Q. Meng, B. Zhu, Y. Zhang, *et al.*, ELECTRONIC COMPONENTS AND MATERIALS, 11, (2012), 43-45.

[59] X.R. Fu, Z.T. Song, X.Z. Duo & C.L. Lin, Journal of Inorganic Materials, 14, (1999), 828-832.

[60] X.Y. Chen, K.H. Wong, C.L. Mak, X.B. Yin, *et al.*, J. Appl. Phys., 91(9), (2002), 5728-5734.

[61] R. Kim, Y. Kim & J.W. Park, Thin Solid Films, 376(1), (2000), 183-187.

Collection @ kmou

Acknowledgement

I would like to express my gratitude to all those who helped me during the writing of this thesis.

My deepest gratitude goes first and foremost to Professor Hong Seung Kim, my supervisor, for his constant encouragement and guidance. He has walked me through all the stages of the writing of this thesis. Without his consistent and illuminating instruction, insightful criticism and expert guidance, this thesis could not have reached its present form.

Second, I would like to express my heartfelt gratitude to Professor Min Yang, Nak Won Jang and Sam Nyung Yi, who teach me so much new knowledge. I am particularly grateful to my thesis committee members for their time and valuable suggestions in guiding and reviewing my work. I am also greatly indebted to all other professors and teachers at the Department of Nano Semiconductor Engineering. Special thanks should go to doctor Jong Hoon Lee, who has put considerable time and effort into investigation on the experiment.

Last my thanks would go to my beloved family for their loving considerations and great confidence in me all through these years. I also owe my sincere gratitude to my fellow classmates who gave me their help and time in listening to me and helping me work out my problems during the difficult course of the thesis. There is also my gratitude to all other friends at Korea Maritime and Ocean University for the friendly environment and emotional supports. I will not forget the time we spent together before and in the future.

dCollection @ kmou